

**BIOINSPIRED MATERIAL DESIGN: MODELING AND OPTIMIZATION OF  
NACRE-LIKE MATERIALS**

A Dissertation

by

NASRA SAID ABDULLAH AL MASKARI

Submitted to the Office of Graduate and Professional Studies of  
Texas A&M University  
in partial fulfillment of the requirements for the degree of

DOCTOR OF PHILOSOPHY

Chair of Committee,	J. N. Reddy
Co-Chair of Committee,	Daniel A. McAdams
Committee Members,	Richard Malak
	Terry Creasy
Head of Department,	Andreas Polycarpou

December 2016

Major Subject: Mechanical Engineering

Copyright 2016 Nasra Said Abdullah Al Maskari

## **ABSTRACT**

Nacre is an inner layer of seashells that is a tough yet stiff natural composite composed of microscopic mineral polygonal tablets bonded by a tough biopolymer. This type of structure is called staggered structure and it has been observed in other biological materials such as bone and teeth. The high stiffness of nacre is known to be due to its high mineral content. In spite of the high mineral content that is mainly ceramic, nacre exhibit high values of toughness. This high value of toughness is explained by its ability to deform past a yield point and develop large inelastic strain over a large volume around defects and cracks. It has been known that the high strain is mainly due to sliding and waviness of the tablets.

Researchers have been motivated by the structure of nacre and its mechanical properties in order to mimic this natural material to create new engineering composites with superior mechanical properties. However, mimicking nacre's remarkable properties, to date, is still a challenge. This is due to fabrication challenges, lack of models that captures the important mechanics and difficulties in selecting the best combination of tablets and matrix materials, and system geometry for optimal mechanical performance (e.g., stiffness, strength and toughness) of the staggered structure. Previous attempts to create analytical models for nacre include tablet sliding but don't account for the waviness of the tablets. In this work, mathematical models for calculating the elastic modulus and toughness of nacre-like material are proposed to account for the waviness of the tablet. In

addition, a multi-objective optimization problem is formulated and solved using an optimization method called ‘genetic algorithm’.

Using the models developed in this work, a better prediction of the elastic modulus and toughness are obtained which agrees with experimental results found in the literature. The multi-objective optimization problem solved here results in a set of optimal solutions that the designers can select according to their preferences. This work will aid in the design and optimization of nacre-like materials that can enhance the performance of ceramic materials in different applications in areas such as material science, biomaterials development, civil, petroleum, biomedical and nanotechnology.

## **DEDICATION**

*To my husband Majid Al-Hinai*

*To my parents Said Al-Maskari and Zuwaina Al-Toqi*

*To my kids Ahmed and Rodaina*

## **ACKNOWLEDGEMENTS**

I would like to express my special appreciation and thanks to my advisors Prof. J. N. Reddy and Prof. Daniel McAdams for their continuous support and mentoring. I would like to thank them for guiding me throughout my research, from selecting the dissertation topic to the end of the work. I would also like to thank my committee members, Dr. Richard Malak and Dr. Teary Creasy, for serving as my committee members and for their insightful comments and feedback. I would like to thank Dr. Richard Malak and his PhD student Edgar Galvan for their assistance in selecting the optimization algorithm. In addition, I am thankful to Edgar Galvan for his help with the optimization toolbox in MATLAB. I am also thankful to Prof. Reddy and Prof. McAdams' group members past and present for their assistance and useful discussions during group meetings

Sincere thanks to my husband for his encouragement, support, patience, love and fruitful discussions throughout my research. In addition, thanks to my parents for their support and love. I am also thankful to my kids for the happiness and joy they bring to my life.

I gratefully acknowledge the financial support of my graduate study at Texas A&M University by Sultan Qaboos University, Muscat 123, Oman.

## TABLE OF CONTENTS

	Page
ABSTRACT .....	ii
DEDICATION .....	iv
ACKNOWLEDGEMENTS .....	v
TABLE OF CONTENTS .....	vi
LIST OF FIGURES .....	viii
LIST OF TABLES .....	x
1. INTRODUCTION.....	1
1.1. Motivation .....	3
1.2. Objective .....	5
1.3. Research Approach .....	6
2. BACKGROUND.....	8
2.1. Bio-Inspired Materials - Biomimetic .....	8
2.2. Biological or Natural Materials.....	9
2.2.1. Properties of Biological Material .....	11
2.2.2. Mollusk Shells.....	11
2.2.3. Nacre .....	19
2.3. Synthetic Nacre-like Materials.....	21
2.4. Modeling of Nacre-like Materials - Shear Lag Model.....	23
2.5. Toughness.....	25
2.5.1. Toughness of Nacre.....	26
2.5.2. Toughness Evaluation .....	27
2.6. Optimization.....	28
2.6.1. Solving an Optimization Problem .....	30
2.6.2. Pareto Solution .....	31
2.6.3. Multi-objective Optimization.....	33
3. LITERATURE REVIEW .....	37
3.1. Stiffness Models.....	37
3.2. Toughness Models.....	38
3.3. Optimization Algorithms.....	39

	Page
4. WAVINESS STIFFNESS MODEL.....	41
4.1. Results and Discussions .....	45
4.2. Dovetail Angle .....	46
5. WAVINESS TOUGHNESS MODEL .....	48
5.1. Quantifying Toughness .....	48
5.2. Crack Resistance Curve (R-curve).....	53
5.3. Results and Discussions .....	55
6. OPTIMIZATION OF NACRE-LIKE MATERIALS .....	61
6.1. Objective Functions.....	62
6.1.1. Stiffness .....	62
6.1.2. Strength .....	62
6.1.3. Toughness.....	63
6.2. Formulation and Solution Approach.....	64
6.2.1. Constraints.....	64
6.2.2. Multi-Objective Formulation .....	66
6.2.3. Implementation and General Description of NSGA II.....	70
6.3. Results and Discussions .....	71
7. CONCLUSIONS, CONTRIBUTIONS AND LIMITATIONS .....	85
7.1. Conclusion.....	85
7.2. Contributions and Limitations .....	87
8. SUGGESTED FUTURE WORK.....	89
REFERENCES.....	90
APPENDICES.....	102
Appendix A .....	102
Appendix B .....	110

## LIST OF FIGURES

	Page
Figure 1. Comparing stiffness and fracture toughness of engineering materials with biological materials. Reprinted with permission from [3].	1
Figure 2. Hierarchical structure of red abalone shell: a) Red abalone shell in centimeters; b) The shell showing the nacreous layer; c) Scanning electron micrograph of a fracture surface in nacre showing the brick and mortar structure; d) Schematic of the tablet. Reprinted with permission from [4].	2
Figure 3. a) Tablet's sliding [2] b) Scanning electron micrographs (SEM) showing the sliding of the tablets and a dovetail-like feature at the end of the tablet [6] c) A few dovetail-like features at the border of the tablets obtained via SEM [7]. Arrows in (b) show direction of sliding. Reprinted with permissions from [2], [6] and [7].	3
Figure 4. Overall road map of the dissertation	7
Figure 5. Various microstructures of mollusk shell. Reprinted with permissions from [8].	17
Figure 6. Hierarchical structure of red abalone. Reprinted with permissions from [77].	18
Figure 7. Stress-strain curve of dry and wet nacre showing the deformation behavior Reprinted with permission from [81].	21
Figure 8. Schematic of 2D unit cell used in the continuum model. Adapted with permission from [3].	24
Figure 9. Typical R-curve for nacre. Adapted with permission from [84]	26
Figure 10. Extrinsic toughening mechanisms observed in nacre. Reprinted with permission from [87]	27
Figure 11. Pareto frontier	32
Figure 12. a) Structure of nacre; b) RVE symmetric about the x-axis; c) A reduced RVE; d) A reduced RVE when a load is applied; e) Forces in a differential element in the overlap region. Reprinted with permission from [113].	42
Figure 13. Schematic showing a crack in nacre with J-integral contours. Reprinted with permission from [79]	48

Figure 14. R-curve for nacre (for two experiments) with logarithmic fit. Reprinted with permission from [79] .....	56
Figure 15. R-curve obtained from waviness toughness model .....	56
Figure 16. R-curve for nacre (for two experiments). Reprinted with permission from [23].....	58
Figure 17. R-curve for nacre (for four experiments) and our model.....	59
Figure 18. R-curve for waviness model for the nacre-like material of Al <sub>2</sub> O <sub>3</sub> /PMMA ....	60
Figure 19. Flat and wavy tablets .....	61
Figure 20. Elastic modulus (E), strength ( $\sigma$ ) and toughness (J) for case I .....	72
Figure 21. Elastic modulus (E), strength ( $\sigma$ ) and toughness (J) for case II.....	72
Figure 22. Elastic modulus (E), strength ( $\sigma$ ) and toughness (J) for case III .....	75
Figure 23. Elastic modulus (E), strength ( $\sigma$ ) and toughness (J) for case IV .....	76
Figure 24. Ashby chart of fracture toughness vs. elastic modulus. Adapted with permission from [124]. .....	79
Figure 25. Ashby chart of fracture toughness vs. strength. Adapted with permission from [124].....	80
Figure 26. Ashby chart of elastic modulus vs. strength. Adapted with permission from [124].....	81
Figure 27. Ashby chart of elastic modulus vs. density. Adapted with permission from [124].....	82
Figure 28. Ashby chart of strength vs. density. Adapted with permission from [124]. ...	83
Figure 29. Fracture toughness vs. density. Adapted with permission from [124]. .....	84

## LIST OF TABLES

	Page
Table 1 Ashby classification of biological materials with examples.....	9
Table 2 Hard biological material.....	10
Table 3 Classification of some mollusk shells. Reprinted with permission from [27] ....	12
Table 4 Comparison of elastic moduli .....	46
Table 5 Solution approach cases .....	66
Table 6 Comparisons of case I and II with experimental values from literature .....	73
Table 7 Optimal design variables data obtained from multi-objective optimization algorithm.....	77
Table 8 Optimal design variables for randomly selected five points .....	77

# 1. INTRODUCTION

Natural or biological materials are made from weak constituents that are combined and structured in such a way that results in outstanding mechanical properties [1]. Stiffness and toughness are often mutually exclusive mechanical properties. Engineering materials are usually either stiff such as some metals or tough such as ceramics but biological materials can be both stiff and tough such as bone and mollusk shells (nacre) as can be seen in Figure 1. This comparison is qualitative not quantitative. Such performance of biological materials is due to the staggered structure in which the stiff tablets are wrapped by a soft ductile interface (or matrix) [2]. In general, stiffness of the staggered structure is due to high content of stiff minerals while the matrix channels the cracks leading to an increase in toughness.

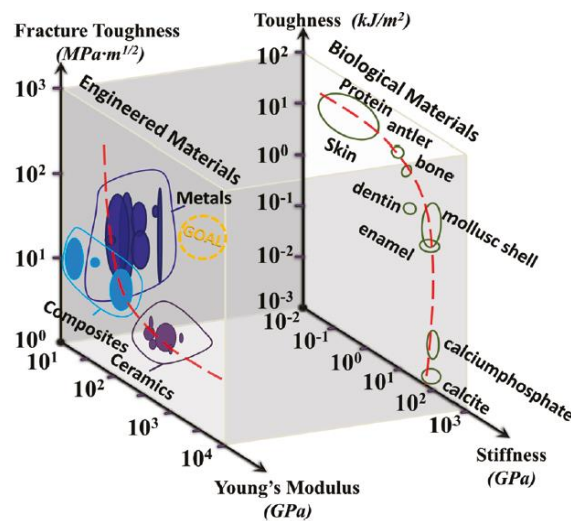


**Figure 1.** Comparing stiffness and fracture toughness of engineering materials with biological materials. Reprinted with permission from [3].

Mollusk shells have a two-layer system to protect themselves from predators. The outer layer of the shell is made of large prismatic calcite grains while the inner layer is made of nacre as shown in Figures 2a and 2b. Nacre, which is known as mother of pearl, is a tough yet stiff natural composite composed of microscopic mineral polygonal tablets bonded by a tough biopolymer. The mineral is calcium carbonate  $\text{CaCO}_3$ , which is 95% of the material while the rest is an organic matrix made from proteins and polysaccharides. The tablets are stacked to form a 3D brick wall structure referred to as a brick and mortar structure. This brick and mortar structure is shown in Figures 2c and 2d.

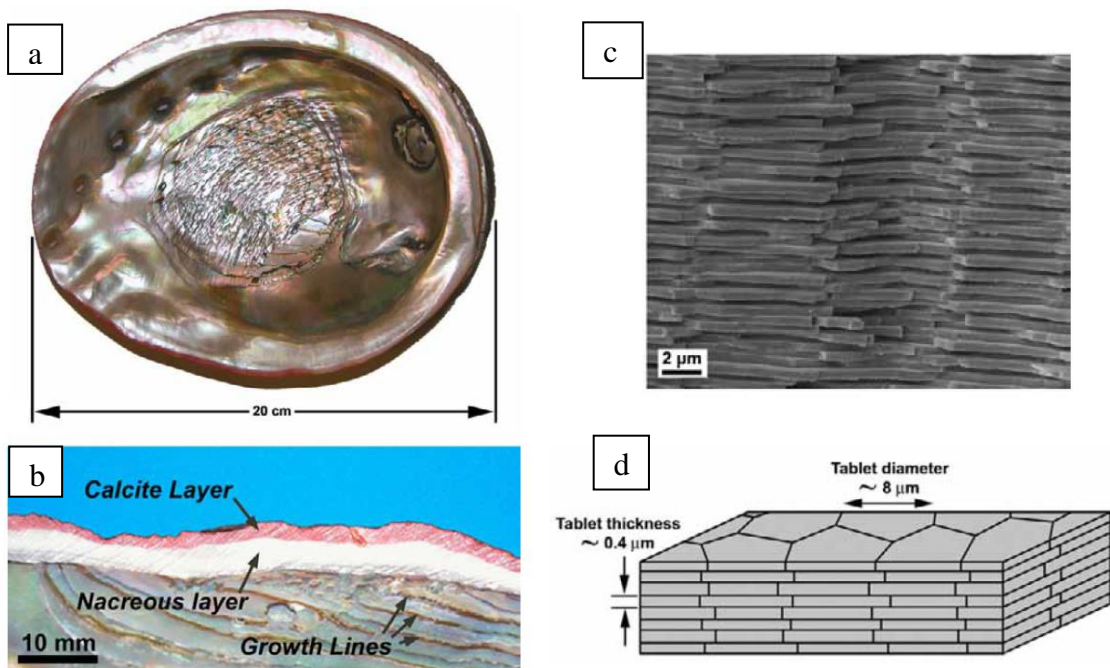


**Figure 2.** Hierarchical structure of red abalone shell: a) Red abalone shell in centimeters; b) The shell showing the nacreous layer; c) Scanning electron micrograph of a fracture surface in nacre showing the brick and mortar structure; d) Schematic of the tablet. Reprinted with permission from [4].

It is noted that the tablets' surface is not flat [4]. There is some wedge geometry or waviness that generates interlocking which spreads energy and increases the toughness of nacre. The waviness functions somewhat as a dovetail joint. The angle is very small to allow sliding and progressive pullout of the tablets [5]. Figure 3 shows the sliding of the tablets as well as the dovetail like feature 'waviness'.

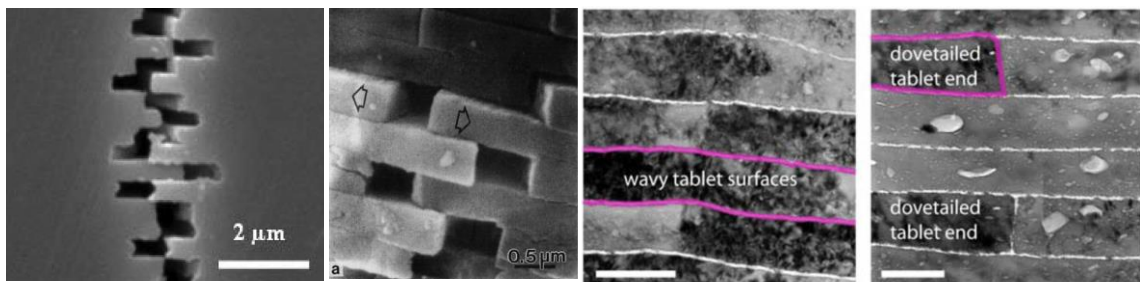


**Figure 3.** a) Tablet's sliding [2] b) Scanning electron micrographs (SEM) showing the sliding of the tablets and a dovetail-like feature at the end of the tablet [6] c) A few dovetail-like features at the border of the tablets obtained via SEM [7]. Arrows in (b) show direction of sliding. Reprinted with permissions from [2], [6] and [7].

### 1.1. Motivation

Nacre has less complex architecture in comparison with other biological materials. This is because nacre's structure is optimized for only mechanical properties since it does not perform sensing, temperature regulating, or other function. Therefore, nacre has been studied greatly in order to mimic its properties into engineering materials. Bio-mimicking nacre has resulted in materials that have toughness much larger than their constituent materials or materials that exhibit similar deformation mechanisms [1, 8].

Despite the significant experimental and theoretical effort in mimicking the mechanical properties of nacre into engineering materials, many challenges exist. First,

models developed to calculate nacre's mechanical properties are very simplified and considered to be one dimensional models. In addition, these models assume the tablets are flats and don't consider the waviness that is contributing to the high toughness observed in nacre. Second, in spite of the existing guidelines for designing of nacre like materials, there is no clear steps of selecting the geometry and material of the staggered structure to produce optimal mechanical performance (e.g., stiffness, strength and toughness). In addition, the improvement in toughness relative to its main constituent is not as great as in nacre. So currently designing of nacre-like materials can be considered to be done by trial and error. Third, many fabrication challenges exists with different fabrication techniques [5, 8-17]. More details about fabrication techniques is shown in section 2.3. In this work, the first two challenges are considered and the fabrication challenges will not be covered.

In summary, the main motivations behind this work are presented in the following points:

- Mimicking the high toughness and stiffness into engineering materials is desired.
- A model/models that predicts the bulk properties from its main constituents is needed.
- Models in literature assumes the tablets are flat and don't account for tablet waviness which is one of the reasons of high toughness observed in nacre.
- Methods of selecting candidate materials is not clear.
- Geometry of staggered structure is not selected for optimality.
- Designing of bio-inspired materials is done currently by trial and error.

- The improvement in toughness relative to its main constituent is not as great as in biological materials

This work will aid in the design of nacre-like materials in which the designer can use the model to predict the mechanical properties (e.g. stiffness and toughness) of different nacre-like materials in order to select the appropriate one. In addition, the optimization algorithm will aid the designer in selecting the optimal geometry and suggest candidate materials of the staggered structure leading to high performance nacre-like materials. Knowing the connections between material's structure and its mechanical properties aids in replacing or improving upon existing ceramic materials useful in areas such as material science, biomaterials development, civil, petroleum and nanotechnology. Nacre-like material can be tough and light suitable for high-efficiency industrial cutting and drilling tools [18]. Nacre-like materials and coatings have been developed for biomedical applications such as development of better performance implant materials that are usually made of brittle ceramic materials. Using nacre-like materials may enhance the strength and toughness properties of implant materials [19]. In addition, researchers are looking into using cement paste, which is concrete's binding ingredient, with the structure and properties of natural materials such as nacre, bone and deep-sea sponge [20].

## **1.2. Objective**

In light of the previous introduction and motivation, the main objectives of this dissertation are as follows:

- Build an improved model of a biological hard material (Nacre) to predict the mechanical properties in order to aid in designing of bio-inspired materials.

- The waviness should be included in the model.
- The model should predict the following mechanical properties.
  - Stiffness
  - Toughness
- The model should be able to predict the optimal material and geometry of the tablets and interface (matrix) to produce the optimal mechanical properties that is optimal stiffness, strength and toughness.

### **1.3. Research Approach**

The overall road map is shown in Figure 4. The work is divided into several major steps as follows:

- Develop a waviness stiffness model to predict the stiffness of the nacre-like composites.
- Develop a waviness toughness model to predict the toughness.
- Develop an optimization algorithm that utilizes the two above models to predict the material and geometry of the staggered structure for optimum toughness and stiffness since these are conflicting properties.



**Figure 4.** Overall road map of the dissertation

In the following section, background information about relevant concepts are illustrated. Following that, a review of related work is given in section 3. Then, the developed stiffness and toughness model are demonstrated in sections 4 and 5, respectively. These models are combined with strength predication into an optimization algorithm as illustrated in section 6. Section 7 includes the conclusion followed by contributions and limitations demonstrated in section 8 and future work shown in section 9.

## **2. BACKGROUND**

This section illustrates some of the main concepts found in the area of bio-inspired materials. Initially, a brief introduction about the field of bioinspired materials also called biomimetic is given in section 2.1. Following that, general information about biological materials and their properties are shown in section 2.2. Section 2.2 also contains a brief introduction about mollusk shells and nacre. Methods commonly used to develop synthetic bio-inspired materials are shown in section 2.3. In addition, the shear lag model which is commonly used to model nacre is discussed in section 2.4. After that, Toughness and toughening mechanisms are discussed in section 2.5. Finally, background information about optimization is illustrated in section 2.6.

### **2.1. Bio-Inspired Materials - Biomimetic**

Bio-inspired materials or biomimetic is an interdisciplinary field where scientists and engineers are trying to learn from nature to create novel improvements in technology. Bio-inspired design is the development and implementation of concepts learned from nature. Generating bio-inspired material and structures has two levels or two approaches. The first is to use concepts from nature using synthetic materials and processing methods. This is more conventional. The second approach is considered to be molecular-based bio-inspired structure design in which bio-inspired processes at molecular level such as self-assembly are used to generate new materials and structures. This is a bottom-up approach where hierarchical complexity of biological materials is included [1, 6].

## 2.2. Biological or Natural Materials

Natural or biological material are made from weak constituents that have evolved hundreds of millions year thus having outstanding mechanical properties [1]. Biological material can be classified based on Wegst and Ashby [21, 22] as ceramics, polymer composites, elastomers and cellular materials. Examples are shown in Table 1.

**Table 1** Ashby classification of biological materials with examples.

Biological material	Main Feature	Example
Ceramic	Composed mainly from minerals	Teeth, bones, shells, diatoms and spicules of sponges
Polymer	-	Ligaments and tendons, silk, hooves of mammals and arthropod exoskeletons
Elastomers	Can have large strains	Skin, muscle, blood vessels and soft tissues in body
Cellular material	Light weight	Wood, cancellous bone, feathers and beak interior

Biological material can also be classified based on its mechanical property into soft and hard material [1]. Hard materials provides skeleton; teeth, nails in vertebrates and exoskeleton in arthropods. Whereas soft materials build skin, muscle, internal organs, etc. Examples of hard biological material are shown in Table 2.

**Table 2** Hard biological material

Hard Biological material	Basic building block	Includes in
Calcium phosphate (hydroxyapatite- $\text{Ca}_{10}(\text{PO}_4)_6(\text{OH})_2$ )	mineral	teeth, bone, antlers
Calcium carbonate (aragonite)	mineral	Mollusk shells ,some reptile eggs
(calcite)	-	Bird eggs, crustaceans, mollusks
Amorphous silica( $\text{SiO}_2(\text{H}_2\text{O})_n$ )	mineral	Spicules in sponges, diatoms
Iron oxide(Magnetite- $\text{Fe}_3\text{O}_4$ )	mineral	teeth in chitons (a weird looking marine worm), bacteria
Collagen	Protein	organic component of bone and dentine, tendons, muscle, blood
Keratin	Protein	bird beaks, horn and hair
Elastin	Protein	skin, lungs and artery walls
Chitin	Polysaccharide	arthropod and insect exoskeletons
Cellulose	Polysaccharide	Plant cell walls

### 2.2.1. *Properties of Biological Material*

Biological material has special features that are not there in mechanical materials such as [1, 23, 24]

- Multifunctional: they can perform more than one function. For example: Bone is forming blood cell and it is a support for the body. Mammal skin is regulating the temperature and protect the internal tissues from environment.
- Hierarchy organization of the structure: Different level, from molecular to macroscopic, have different architectures and they are held together by specific interactions between components.
- Self-healing; most biological material structures can repair themselves if damaged with exceptions to teeth, cartilage and brains.
- Self-organization and Self-assembly. Self-assembly is when the molecules arrange themselves under certain conditions into specific arrays.
- Low density: the density of structural natural materials rarely exceed  $3 \text{ gm cm}^{-3}$  since natural materials doesn't contain heavy elements such as metals. Synthetic structural materials are often having densities in the range of  $4\text{-}10 \text{ gm cm}^{-3}$ .
- Having a wide range of young moduli and strengths.
- Energy saving.

### 2.2.2. *Mollusk Shells*

Mollusk shells are two layer systems made of calcium carbonate and organic macromolecules. Hence, mollusk shells are considered to be composites. The calcium carbonate can be in crystal form of calcite or aragonite. The organic macromolecules are

mainly proteins and polysaccharides. There are different classes of mollusks shells with about 60,000 species. The most common classes are gastropods and bivalves with about 35,000 and 10,000 species, respectively [25, 26]. Gastropods include conch shell, top shell and abalone shell. Bivalves includes clams, oysters and freshwater mussels. Classification of some mollusk shells is shown in Table 3.

**Table 3** Classification of some mollusk shells. Reprinted with permission from [27]

Class	Family	Genus	Specie	References
<b>Bivalves</b>	Meretricinae	Meretrix	Meretrix lusoria	Fleischli et al. [28]
	Mytilidae	Bathymodiolus	Bathymodiolus azoricus	Machado et al. [29]
		Perna	Perna canaliculus (green mussel)	Leung and Sinha [30] Pokroy et al. [31] Moshe-Drezner et al. [32]
		Modiolus	Modiolus modiolus	Currey [33]
	Nuculidae	Nucula	Nucula nitidosa	Cartwright and Checa [34] Checa et al. [35, 36]
	Pinnidae (pen shell)	Atrina	Atrina pectinata	Cartwright and Checa [34]
			Atrina rigida	Nudelman et al. [37]

**Table 3** Continued

Class	Family	Genus	Specie	References
			<i>Atrina vexillum</i>	Currey [33]
	Pteriidae	Pteria	<i>Pteria avicula</i>	Cartwright and Checa [34] Cartwright et al. [38]
			<i>Pteria hirundo</i>	Cartwright and Checa [34]; Cartwright et al. [38]
			<i>Pteria penguin</i>	Fleischli et al. [28]
		Pinctada (pearl oysters)	<i>Pinctada maxima</i>	Stempfle´ and Brendle´ [39]; Stempfle´ et al. [40]; Wang et al. [41].
			<i>Pinctada margaritifera</i>	Chateigner et al. [42]; Checa et al. [36]; Currey [33]; Currey et al. [43]; Jackson et al. [44]; Rousseau et al. [45]
			<i>Pinctada</i> sp.	Currey [33]
	Tellinidae	Tellinella	<i>Tellinella asperrima</i>	Ren et al. [46]
	Unionidae	Anodonta	<i>Anodonta cygnea</i> (swan mussel)	Cartwright and Checa [34]; Currey [33]; Machado et al. [29]

**Table 3** Continued

Class	Family	Genus	Specie	References
		Hyriopsis	Hyriopsis schlegeli	Song et al. [47]
		Lamprotula	Lamprotula fibrosa	Sun and Tong [48]
<b>Gastropods</b>	Calliostomatidae	Calliostoma	C.zizyphinum	Cartwright and Checa [34]
	Haliotidae	Haliotis (abalone)	Haliotis asinina	Cartwright and Checa [34]
			Haliotis fulgens (green abalone)	Lin and Meyers [49]; Meyers et al. [50, 51]
			Haliotis genus	Heinemann et al. [52]
			Haliotis iris	Song et al. [53, 54]
			Haliotis laevigata (greenlip abalone)	Blank et al. [55]; Heinemann et al. [52]
			Haliotis rufescens (red abalone)	Barthelat et al. [4, 56]; Bezares et al. [57, 58]; Fleischli et al. [28]; Fritz et al. [59]; Li et al. [60, 61];

**Table 3** Continued

Class	Family	Genus	Specie	References
				Lin et al. [62]; Lin and Meyers [49, 63]; Katti et al. [64, 65]; Menig et al. [66]; Meyers et al. [67]; Mohanty et al. [68]; Schaffer et al. [69]; Verma et al. [70]; Wang et al. [41]; Yao et al. [71]; Yourdkhani et al. [72]; Zaremba et al. [73]
			unkonwn	Meyers and Chawla [67]
	Pleurotomariidae	Perotrochus	Perotrochus caledonicus	Checa et al [36]
	Strombidae	Strombus	Strombus gigas	Menig et al [74]
	Trochidae	Gibbula	Gibbula pennanti	Cartwright and Checa [34]
			Gibbula umbilicalis	Cartwright and Checa [34]
		Trochus	Trochus niloticus	Bruet et al. [75]; Currey [33]

**Table 3** Continued

Class	Family	Genus	Specie	References
			(top shell)	
	Turbinidae	Bolma	Bolma rugosa	Cartwright and Checa [34]
		Turbo	Turbo marmoratus	Chateigner et al. [42]; Currey [33]
<b>Cephalopods</b>	Nautilidae	Nautilus	Nautilus pompilius	Currey [33]
<b>Monoplacophora</b>	Neopilinidae	Veleropilina	Veleropilina zografi	Checa et al. [36]

Mollusk shells can have different type of structures at microscale such as; crossed-lamellar, foliated, prismatic, homogeneous, and sheet nacre and columnar nacre [76]. The structures are shown in Figure 5. Nacreous structures are found to be stronger than non-nacreous structures [76]. Therefore, it the most studied type of layer although is not the most common. Columnar nacre is generally found in gastropods. The tablets in columnar nacre are arranged in columns with defined overlap regions. Sheet nacre are generally found in bivalves. The arrangement of the tablets is sheet nacre is more random and the overlap region can't be distinguished easily.

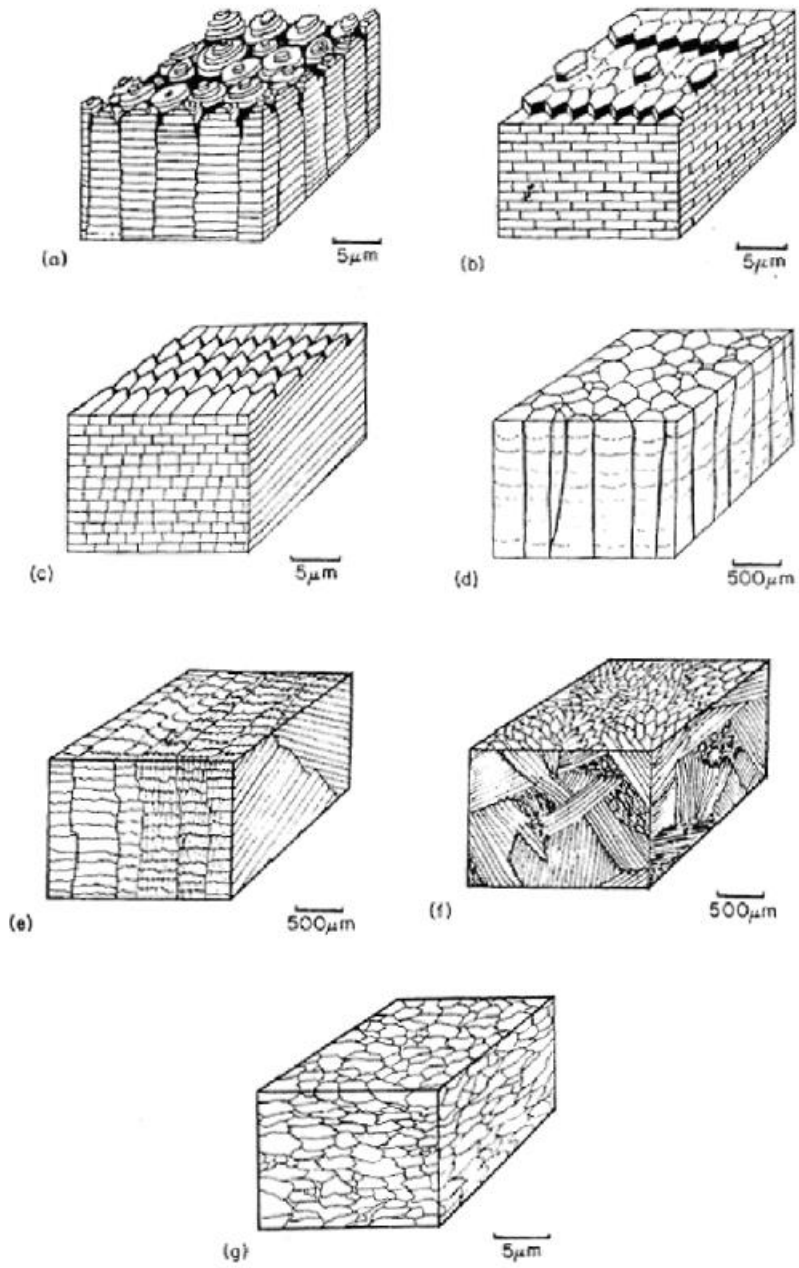


**Figure 5.** Various microstructures of mollusk shell. Reprinted with permissions from [8].

In this work, nacre from red abalone will be considered which has a columnar structure. The hierarchical structure of red abalone is shown in Figure 6. It has five levels of hierarchical structure from nano to macro structural length scales.

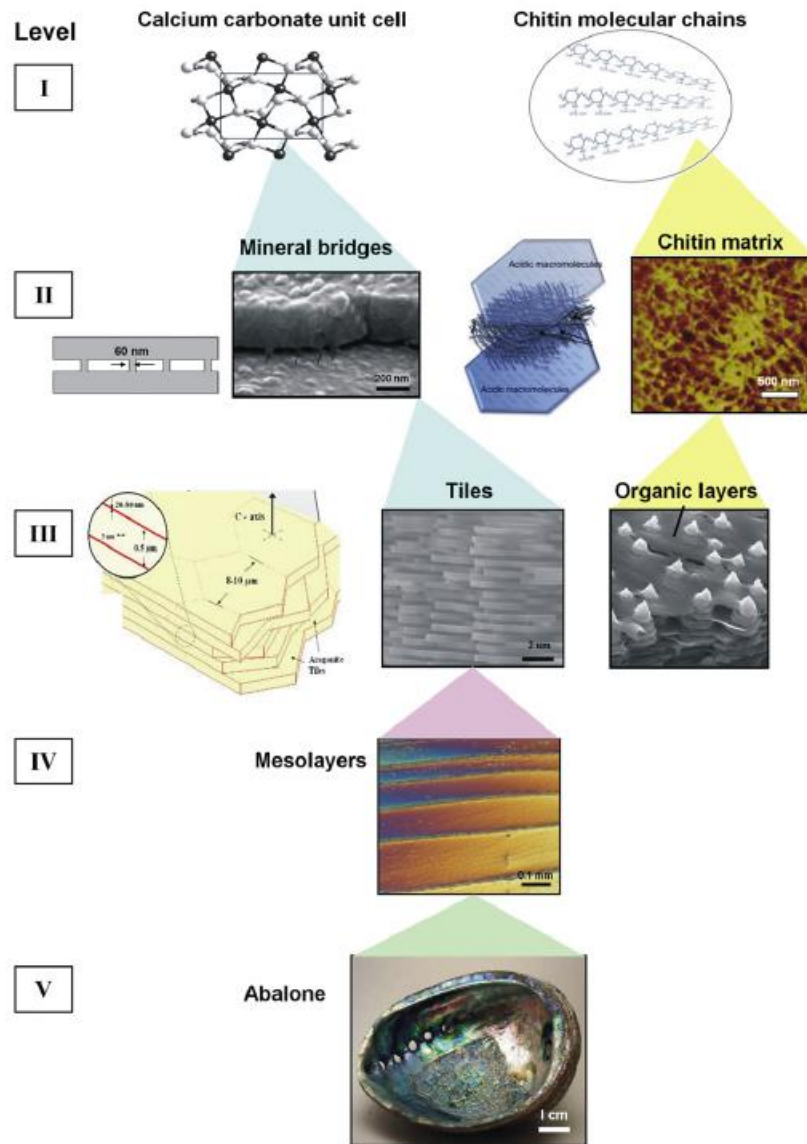


**Figure 6.** Hierarchical structure of red abalone. Reprinted with permissions from [77]

It was suggested that having these levels will allow the researches to analyze the deformation and failure mechanisms at different levels [77]. This is crucial since once the deformation and failure mechanisms are identified they can be translated/mimicked into engineering materials. However, the impact of nanostructure on the modulus and strength was thought to be significant but it has been shown to have a minimal impact [56, 78]. The microstructure have been shown to be contributing the most to high toughness and stiffness observed in nacre [23, 79]. Therefore, the microstructure of red abalone which is Nacre is considered. Mollusk shells is a lightweight and tough armor system. Thus it has inspired the design of armor systems used for protections in body-armor applications [25, 26, 80].

### 2.2.3. *Nacre*

Nacre is, as well, a two layer system composed of about 95% mineral of calcium carbonate and 5 % organic material. The calcium carbonate is in the form of aragonite and the organic material is made of protein and polysaccharides. The mineral is in the shape of polygonal tablets of 5-15  $\mu\text{m}$  in diameter and thickness of 0.5- 1  $\mu\text{m}$ . These tablets are arranged into three dimensional brick walls. The tablets have some waviness that can be observed using optical microscopy, scanning probe microscopy, and scanning and transmission electron microscopy as shown in Figure 3. It is important to consider the function of nacre prior to discussing its mechanical behavior and performance. External loads from predators, rocks or debris displace by currents or waves results in bending of the shell which translates into tension in the inner nacreous layer [5]. The outer calcite

layer of the shell may crack if sever load is applied and the integrity of the shell will be maintained by the nacreous layer [78].

Various experimental tests were performed at different length scales in order to measure the mechanical properties of nacre. Bulk mechanical testing includes uniaxial tension [4, 33, 79], uniaxial compression [56, 66], three and four point bending [41, 44] , and simple shear tests [4]. Microscale and nanoscale indentation tests were also performed in order to obtain the mechanical response of individual components of nacre. Tested samples can be wet or dry. Wet means the sample were hydrated by either soaking in water and it could mean that the sample were taken from the sea and reserved in water until measurements time. Dry nacre indicates samples were not kept in water and left on ambient conditions. Dry nacre behaves like pure aragonite which is similar to a monolithic ceramic and fails in a brittle fashion. Wet nacre exhibit linear elastic behavior followed by a region of high inelastic strain where the material hardened and deformation is spread through the sample until tablets fails by pullout. Stress-strain curves of dry and wet nacre are shown in Figure 7. Measurements of dry and wet nacre showed that the toughness of wet nacre is higher than that of dry ones. High toughness is obtained in the expense of strength and stiffness since the stiffness and strength of wet nacre is lower than that of dry nacre. Generally, the effect of water is to increase the ductility and toughness due to the inelastic deformation. In this work, wet nacre is of interest and will be considered [4, 44].

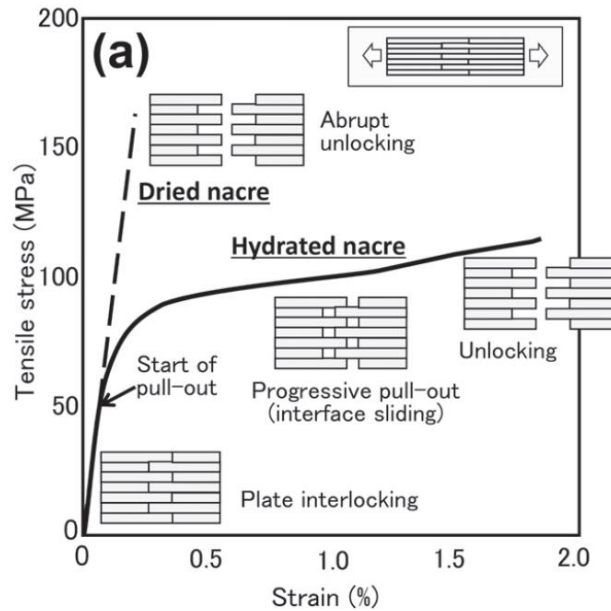


**Figure 7.** Stress-strain curve of dry and wet nacre showing the deformation behavior Reprinted with permission from [81].

Nacre exhibit some ductility with large strain at failure although it is mainly made of a ceramic material.

This is due to the deformation mechanism that acts at microscale. The interface start to yield when the shear strength of the interface is reached. Then the tablets slide on one another creating local deformation. This local deformation spreads over large volumes throughout the specimen creating large strains at macroscale. The tablets pullout once the potential sliding sites are exhausted.

### 2.3. Synthetic Nacre-like Materials

Numerous materials inspired from nacre have been developed over the past 20 year. Innovative fabrication and processing techniques includes [5, 10, 19, 26] :

- Layer by layer deposition which is a simple and versatile method of producing thin films by alternately immersing a charged substrate into two solutions of oppositely charged polyelectrolytes
- Covalent self-assembly or bottom-up approach (bottom-up colloidal assembly): an organic phase provides a template for inorganic crystals to nucleate and grow from supersaturated solution
- Electrophoretic deposition: a technique suitable for the production of nanocomposites in a low-cost approach that allows novel and complex material combinations
- centrifugal deposition process
- shearing cylinders
- Template inhibition: consists of the mineral deposition from solution onto a well-ordered two-dimensional structure of a self-assembled film on solid or liquid substrates
- sedimentation and dipping
- in situ polymerization into porous ceramics
- molecular scale self-assembly and bio-mineralization
- Ice-template sintering of alumina powders.
- Laser engraving technique

Many of these techniques duplicate several features of natural nacre such as unidirectional micro mineral tablets with high aspect ratio embedded in softer, ductile

polymer as a matrix. Nevertheless, they are suitable for small scale and laboratory specimens except for new promising techniques such as 3D printing [17].

#### **2.4. Modeling of Nacre-like Materials - Shear Lag Model**

The amazing performance of nacre and other hard biological materials, such as teeth, collagen fiber, spider silk and cellulose fiber is due to its brick-wall structure known as staggered structure that provides attractive combination of stiffness, strength and toughness. The well-known shear lag model is widely used to model the behavior of Nacre and it concerns with the transfer of tensile stresses from the matrix to the platelets via the interfacial shear stress. One of the earliest model demonstrated by Kotha [82] is based on the following assumptions:

- The platelets are assumed to be rectangular in shape and have a uniform width and isotropic.
- The platelets are fully overlapped and uniformly arranged
- The platelets carry the axial stresses and the stress is transferred from one platelet to the other by shear
- The matrix at the ends of the platelets contributes little to the stress transfer
- Shear stress is assumed to be constant in the matrix on the sides of the platelets
- The deformation and stresses perpendicular to the applied stresses direction are ignored
- In deriving the elastic modulus, bonding is assumed perfect and no interface is present
- Residual stress effects are neglected

- The matrix is assumed to be elastic-perfectly plastic in shear and fails when ultimate shear strain is reached.
- The shear stress is assumed to be uniform

Figure 7 shows the 2D unit cell (RVE) used in this model. The overlap length is  $L$ , the thickness of the tablet is  $b$  and the thickness of the matrix is  $h$ . In biological staggered structure the load is transferred between the tablets through shear stress in the overlapped region and in order to simulate the load transfer mechanism, a tensile stress is applied at the right of the top tablet and the left end of the bottom tablet was fixed in the axial direction.

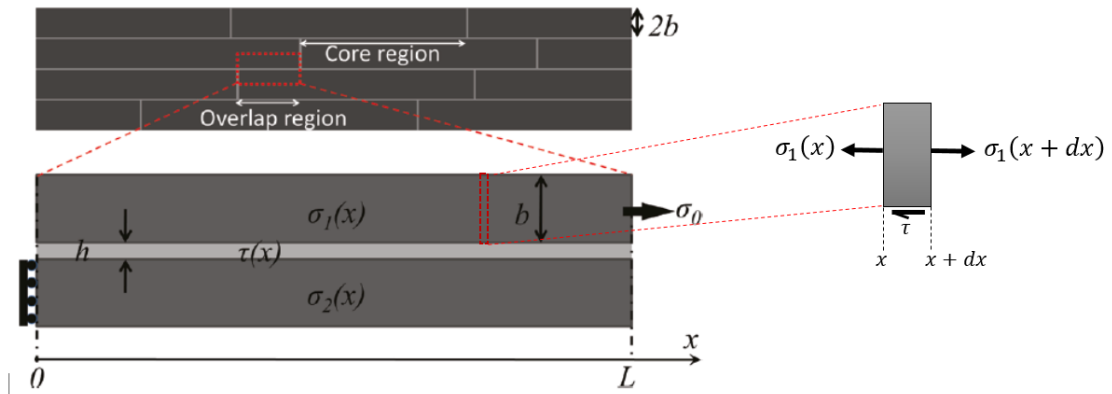


**Figure 8.** Schematic of 2D unit cell used in the continuum model. Adapted with permission from [3].

The effective elastic modulus of the composite is given by

$$E = \frac{2E_t \lambda b L}{(2b + h) \left[ \lambda L + 2 \coth\left(\frac{\lambda L}{2}\right) \right]} \quad (2.1)$$

Where  $\lambda = \sqrt{2G/Ebh}$

## 2.5. Toughness

Nacre is 3000 times, in energy terms, tougher than its main constituent aragonite [44]. This amount of amplification has not been achieved in synthetic nacre-like materials. The best nacre-like material is 700 times tough than its main constituent [10]. The high toughness achieved by nacre is mainly due to toughening mechanisms. Toughening mechanisms can be classified based on the scale in which they occur. It has been shown that the microscale toughening mechanisms, not the Nano-scale ones [56, 78], are responsible for high values of toughness observed in nacre. Toughening mechanisms can also be classified into extrinsic and intrinsic mechanisms [83]. Intrinsic mechanisms operate ahead of crack tip to prevent damage mechanisms such as cracking or debonding which is commonly found in metals. Extrinsic mechanisms act on the wake of the crack, the area behind the crack tip, to reduce the stress intensity at the crack tip and thus resisting the crack growth. Extrinsic mechanisms result in crack-resistance curve (R-curve) which implies that these materials develop most of their toughening during crack growth, not during crack initiation. Typical R-curve is shown in Figure 9 which indicates that the toughness is increased with crack extension until it reaches a steady state value where no further toughening is obtained with crack growth.

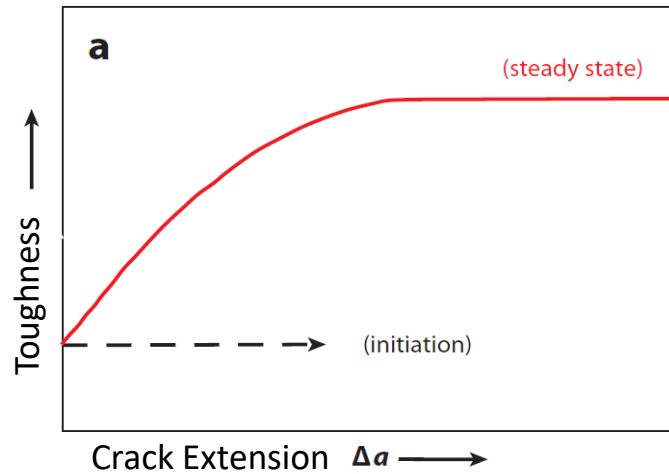


**Figure 9.** Typical R-curve for nacre. Adapted with permission from [84]

### 2.5.1. Toughness of Nacre

The main extrinsic toughening mechanisms that are observed in nacre are crack deflection [44, 85], crack bridging [85] and viscoplastic-energy dissipation in volumes of materials around cracks in an area where the tablets slides onto one another known as a process zone [23, 79, 86]. These toughening mechanisms operate at microscale due to tablet sliding inducing energy dissipation. Additionally due to the waviness in terms of dovetail feature that allows for progressive pull-out and causes hardening and spreading of nonlinear deformation [5]. Figure 3 shows the sliding of the tablets as well as the dovetail like feature ‘waviness’.

The schematic illustration of toughening mechanisms are shown in Figure 10. In crack deflection, the main crack is deflected along the weak planes parallel to the loading direction. The deflected crack is thus trapped leading to increased toughness and damage tolerance. Crack bridging occurs when mineral tablets are not completely pulled out. Thus

the shear stress between the tablets causes the crack to close. The process zone consists of a frontal zone and a wake. The frontal zone is the area in front of the crack tip while the wake is the area behind the crack tip. Sliding and inelastic deformation occurs at the interface in frontal zone. However, the contribution of crack deflection to nacre's toughness is not quantified to date. In addition, crack bridging has a minimum contribution comparing to toughening caused by process zone due to the short sliding distance [79].

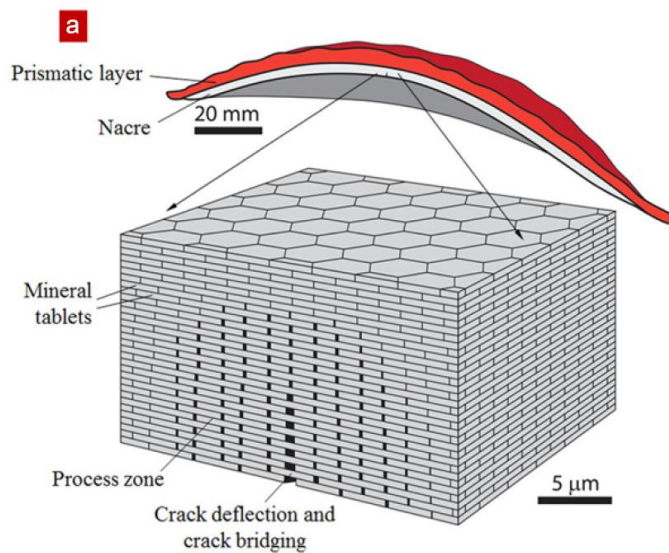


**Figure 10.** Extrinsic toughening mechanisms observed in nacre. Reprinted with permission from [87]

### 2.5.2. Toughness Evaluation

In order to evaluate toughness, fracture mechanics is used. Linear elastic fracture mechanics can't be used because the staggered structure of nacre contains a source of plasticity. This plasticity is due to ductility of the biopolymer. Consequently, nonlinear elastic fracture mechanics is used. In nonlinear elastic fracture mechanics specifically in

elastic-plastic fracture mechanics there are two parameters to measure fracture toughness; crack opening displacement and  $J$ -integral. In this work,  $J$ -integral is used.  $J$ -integral is the change in potential energy of deformation occurring during infinitesimal growth of a crack in a nonlinear elastic material. ' $J$ ' is equivalent to the fracture energy ' $G$ ' in linear elastic fracture mechanics.

## 2.6. Optimization

Optimization is the process of obtaining the best design or element that will satisfy the defined constraints. Optimization starts with defining the design variables, formulating the objective function in terms of maximisation or minimisation and then, specifying the constraints. The objective function and the constraints are in terms of the design variables. Optimization problems can be categorised in terms of problem formulation into single and multi-objective problems. A single objective optimization is concerned with either maximizing or minimizing a function. The definition of the single objective optimization problem is as follows:

Definition .1: A general single optimization problem includes a set of  $n$  parameters (design or decision variables), a single objective function, and a set of  $m$  constraints. Objective function and constraints are functions of the design variables. The optimization goal is to

$$\text{Max or Min } y = f(x)$$

$$\text{Subjected to } \mathbf{e}(x) = (e_1(x), e_2(x), \dots, e_m(x)) \leq \mathbf{0}$$

$$\text{Where } \mathbf{x} = (x_1, x_2, \dots, x_n) \in \mathbf{X}$$

$$y \in \mathbf{Y}$$

And  $\mathbf{x}$  is the decision vector,  $\mathbf{y}$  is the objective function,  $\mathbf{X}$  is denoted as the decision space and  $\mathbf{Y}$  is called the objective space. The constraints  $\mathbf{e}(\mathbf{x}) \leq \mathbf{0}$  determine the set of feasible solutions.

However, in real engineering problems the objective function is usually not single. In bioinspired material design it is always desirable to increase the stiffness, strength and toughness of the staggered structure. These are conflicting objectives hence there is a need to reformulate the optimization problem as a multi-objective optimization which can handle these conflicting objectives. The definition of multi-objective formulation is shown below:

Definition .2: A general multi-objective optimization problem includes a set of  $n$  parameters (design or decision variables), a set of  $k$  objective functions, and a set of  $m$  constraints. Objective function and constraints are functions of the design variables. The optimization goal is to

$$\text{Max or Min } \mathbf{y} = \mathbf{f}(\mathbf{x}) = (f_1(x), f_2(x), \dots, f_k(x))$$

$$\text{Subjected to } \mathbf{e}(\mathbf{x}) = (e_1(x), e_2(x), \dots, e_m(x)) \leq \mathbf{0}$$

$$\text{Where } \mathbf{x} = (x_1, x_2, \dots, x_n) \in \mathbf{X}$$

$$\mathbf{y} = (y_1, y_2, \dots, y_k) \in \mathbf{Y}$$

And  $\mathbf{x}$  is the decision vector,  $\mathbf{y}$  is the objective vector,  $\mathbf{X}$  is denoted as the decision space and  $\mathbf{Y}$  is called the objective space. The constraints  $\mathbf{e}(\mathbf{x}) \leq \mathbf{0}$  determine the set of feasible solutions.

Note that multi-objective optimization problem is sometimes solved by reducing the problem to a single objective optimization problems by methods such as sum weight

and product sum [88] where each objective is given a weight representing its importance. It can also be solved by reducing the problem into a vector of single objective problems called scalarizations such as epsilon-constraint method.

### *2.6.1. Solving an Optimization Problem*

Over the years, a lot of methods were developed to solve optimization problems. These methods can be classified as exact, heuristic and meta-heuristic methods. Exact methods are based on calculus such as dynamic programming, integer programming, mixed integer programming and nonlinear programming. Heuristic methods are techniques for solving, learning and discovery based on experience. They require less computation time which is an advantage over the exact algorithms. They have been used to make quick estimates and preliminary process design which is one of its main limitations. Heuristic techniques can be constructive algorithms such as greedy algorithm or local search methods such as hill-climbing. The third classification is meta-heuristic methods. ‘Meta’ means ‘beyond, in upper level’. Meta-heuristics are strategies that guide the search process and can search a very large range of candidate solutions since they make few or no assumptions about the problem. They do not guarantee an optimal solution hence some of them implement a stochastic optimization. Examples of meta-heuristic techniques are

- Evolution strategies by Rechenberg and Schwefel (1965)
- Evolutionary Programming by Fogel (1966)
- Genetic Algorithm by Holland (1975)
- Simulated Annealing by S. Kirkpatrick, C.D. Gellatt and M.P. Vecchi (1983)

- Tabu Search by Glover (1986)
- Random search by Anatoly Zhigljavsky (1991)
- Ant Colony optimization by Dorigo (1992)
- Particle Swarm Optimization by Eberhart and Kennedy (1995)
- Differential Evolution by Storn and Price (1997)

Single objective optimization problems results in one optimal solutions while multi-objective optimization problems results in a set of optimal solutions called Pareto frontier or simply Pareto solution. More information about Pareto solution is discussed in the following section.

#### *2.6.2. Pareto Solution*

The solution to multi-objective optimization problem results in a set of optimal solutions called Pareto frontier that gives the designers the flexibility to select according to their preferences. For instance, if it is desired to maximize two objective functions (for example, toughness and stiffness). The resulted Pareto frontier is shown in Figure 11.

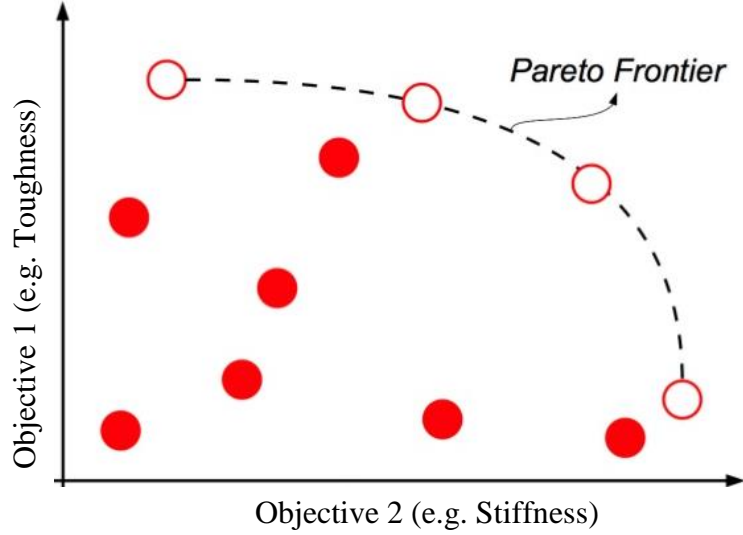


**Figure 11.** Pareto frontier

The Pareto frontier contains non-dominated solutions which means all of the points connected by Pareto frontier have a trade-off associated with toughness vs. stiffness, so none is clearly superior to the others. That is to say, none of the solutions will simultaneously increase the two objectives (toughness and stiffness) [89]. Pareto Dominance can be defined as follows

Definition. 3: For any two decision vectors  $\mathbf{a}$  and  $\mathbf{b}$

$$\begin{aligned}
 \mathbf{a} > \mathbf{b} \text{ (} \mathbf{a} \text{ dominates } \mathbf{b} \text{)} & \quad \text{iff } \mathbf{f}(\mathbf{a}) > \mathbf{f}(\mathbf{b}) \\
 \mathbf{a} \succeq \mathbf{b} \text{ (} \mathbf{a} \text{ weakly dominates } \mathbf{b} \text{)} & \quad \text{iff } \mathbf{f}(\mathbf{a}) \geq \mathbf{f}(\mathbf{b}) \\
 \mathbf{a} \sim \mathbf{b} \text{ (} \mathbf{a} \text{ is indifferent to } \mathbf{b} \text{)} & \quad \text{iff } \mathbf{f}(\mathbf{a}) \not\geq \mathbf{f}(\mathbf{b}) \wedge \mathbf{f}(\mathbf{b}) \not\geq \mathbf{f}(\mathbf{a})
 \end{aligned}$$

*The definitions for a minimization problem ( $<$ ,  $\leq$ ,  $\sim$ ) are analogical.*

Based on the definition of Pareto Dominance, the definition of Pareto Optimal can be introduced for multi-objective optimization. A solution is Pareto optimal if it cannot be

improved without causing a degradation in at least one of the other objectives. The definition of Pareto Optimality is given below.

Definition. 4: A decision vector  $\mathbf{x} \in \mathbf{X}_f$  is said to be non-dominated regarding a set  $\mathbf{A} \subseteq \mathbf{X}_f$  if

$$\nexists \mathbf{a} \in \mathbf{A} : \mathbf{a} \succ \mathbf{x}$$

If it is clear within the context which set  $\mathbf{A}$  is meant, it is simply left out. Moreover,  $\mathbf{x}$  is said to be Pareto Optimal if  $\mathbf{x}$  is non-dominated regarding  $\mathbf{X}_f$

### 2.6.3. Multi-objective Optimization

Multi-objective optimization is the process of simultaneously optimizing two or more conflicting objectives subject to certain constraints. Multi-objective optimization can be also classified into four classes based on how the decision's maker or designers articulate preferences. Preferences indicates the ordering or relative importance of objectives. The four classes are no preference methods and a priori, a posteriori and interactive articulation of preferences methods. In the no preference methods neutral compromise solution is identified without preference information since no designer or decision maker is expected to be available [90]. In the priori methods, the user indicates the relative importance of the objective functions before running the optimization algorithm. In the posteriori methods, a set of mathematically equivalent solutions are obtained in which the designers can select from. In the interactive articulation of preferences method, the designer is continually providing input during the run of the algorithm.

Posteriori methods can be categorized into two categories: mathematical programming based algorithm and evolutionary algorithms. In mathematical programming based algorithm, one Pareto optimal solution is produced by the algorithm each run. Examples of mathematical programming based algorithm are

- Normal boundary interaction (NBI) [91]
- Modified normal boundary intersection (NBI<sub>m</sub>) [92]
- Normal constraint (NC) [93, 94]
- Successive Pareto optimization (SPO) [95]
- Directed search domain (DSD) [96]

In these methods the multi-objective optimization is reformulated into several single objective optimization problem, known as scalarizations. The solution results in a Pareto optimal solution.

Evolutionary algorithms produces a set of Pareto optimal solution in one run. Evolutionary algorithms uses concepts such as reproduction, mutation, recombination and selection inspired by the biological model of evolution. Evolutionary algorithms use a population approach to search for a solution which is useful in a sense that the search is parallel and it has the ability to avoid being trapped in a local optimal solution. Examples of evolutionary algorithms are

- Genetic algorithm
- Genetic programming
- Evolutionary programming
- Gene expression programming

- Evolution strategy
- Differential evolution
- Neuro evolution
- Learning classifier system

One of the most popular evolutionary algorithm is genetic algorithm. Genetic algorithms are population based meta-heuristic optimization algorithms. Genetic Algorithm, and their stochastic various variants, have been well addressed in the literature and it has been successfully used in complex optimization problems [89]. Genetic algorithm is suitable when large numbers of design variables are included and the dimensionality of the problem (i.e. the number of objective functions) is increased. The objective function in genetic algorithm does not need to be continuous nor differentiable unlike many other traditional optimization methods since genetic algorithm uses rank, also called fitness, scores obtained from objective functions without other derivative or auxiliary information. In genetic algorithm, preferences need not to be specified. Thus a set of optimal solution can be generated in which the designer has the opportunity of looking at various available solutions. The general description of genetic algorithm is as follows. A population is generated randomly and is iteratively evolved over many generations. A fitness function and a selection strategy are used to determine the survival of candidates (including their offspring) from generation to generation. The fitness function evaluates each candidate according to how close it is to the desired outcome. The selection strategy favors the better solutions. Over time, the quality of the solutions in the

population should improve. Once a good enough solution is obtained the evolution can be terminated.

Algorithms based on Genetic Algorithms are

- Niched Pareto Genetic Algorithm -NPGA (1994) [97]
- Niched Pareto Genetic Algorithm NPGA II (2001) [98]
- Non-dominated Sorting Genetic Algorithm - NSGA (1994) [99]
- Non-dominated Sorting Genetic Algorithm II - NSGA II (2000) [100]
- Micro-Genetic Algorithm - Micro-GA - (2001) [101]
- Micro-Genetic Algorithm 2 - Micro-GA2 (2003) [102]
- Multi-Population Genetic Algorithm - MPGA - (2003) [103]
- Pareto Efficient Global Optimization -ParEGO - (2006) [104]

Many software have genetic algorithm as part of their optimization toolbox.

MATLAB is one of the popular programs that have built in functions based of genetic algorithm that engineers can use to solve multi-objective engineering optimization problems. MATLAB multi-objective optimization is based on no-dominated sorting genetic algorithm II (NSGA II). NSGA II was introduced by Deb et al. [100]. NSGA II is relatively computationally fast and has better performance than no-dominated sorting genetic algorithm (NSGA) and other algorithms [105].

### 3. LITERATURE REVIEW\*

The review is divided into three sections; Stiffness Models, toughness models and Optimization algorithm. The division is based on the three main tasks discussed in the research approach section. In each section the relevant work in the literature are discussed.

#### 3.1. Stiffness Models

The remarkable performance of nacre and other hard biological materials, such as teeth, collagen fiber, spider silk, and cellulous fiber, is due to its staggered brick-wall structure that provides an attractive combination of stiffness, strength, and toughness. The well-known shear lag model is widely used to model the behavior of nacre [44, 82, 106]. The shear lag model concerns the transfer of tensile stresses from the matrix to the tablet via the interfacial shear stress. One of the earliest models was demonstrated by Kotha, Li, and Guzelsu [82], who proposed a micro-mechanical model for the elastic deformations of nacre that calculates the elastic modulus. Zhang et al. [107] investigated the mechanical properties (i.e. elastic modulus, strength, and failure strain) of a staggered structure with different tablet distributions. In their work, Zhang et al. calculated the critical tablet aspect ratio which distinguishes between tablet and matrix failure with the assumption of a uniform shear stress distribution. Bar-On and Wagner [108, 109] proposed an accurate and compact formula for the effective modulus of staggered composite structures built on

---

\*Part of this section is reprinted with permission from, "Modeling of a biological material nacre: Waviness stiffness model," by Authors' N. S. Al-Maskari, D. A. McAdams, and J. N. Reddy, 2017. *Materials Science and Engineering: C*, vol. 70, Part 1, pp. 772-776, Copyright 2016 by Elsevier B.V.

a generic tablet architecture. Begley and coworkers [110] introduced different failure mechanisms for identical and uniformly distributed tablets lifting the assumption of a uniform shear stress. Wei and coworkers [3] proposed an optimal overlap length of identical and uniformly distributed tablets in elastic and plastic regimes. Dutta et al. [111] developed an analytical model for a staggered structure considering dynamic time dependent loading and computed the optimal overlap length in dynamic regime. Recently, Sakhavand and Shahsavari [112] developed a more generalized model considering non-identical tablets properties. However, all of these models assume that the tablets are flat and do not account for the waviness of the tablets. In this work, a model is developed to account for tablet waviness. Thus, an understanding of the impact of tablet waviness on bulk material properties can be understood, predicted, and designed into a nacre-like engineered material [113].

### **3.2. Toughness Models**

Few models exist that take into account specific toughening mechanisms. Okumura and de Geenes [114] used Griffith criteria to calculate the fracture energy ' $G$ '. Gao [115, 116] developed a simple estimation of fracture energy based on their developed tension-shear chain model combined with Dugdale-type cohesive zone model. The tension-shear chain model is a one-dimensional serial spring system in which the tablets are in tension and the interface is in shear. The fracture energy, in the Dugdale-type cohesive zone model, is calculated based on  $J$ -integral. Shao et al. [117] developed a discontinuous crack-bridging model. The model measures the toughness due to bridging toughening mechanism in terms of stress intensity factor. Barthelat and Rabiei [23] used

a  $J$ -integral approach to calculate the fracture toughness of nacre considering bridging and process zone toughening mechanisms. However, the toughness values due to process zone considers only the sliding of the tablets and assumes the tablets are flat. It has been shown that there are some waviness on the tablets that generate progressive tablet locking, strain hardening and spreading of large deformation over large volumes. Thus high value of toughness is achieved [4, 5]. In all above reviewed models, the effect of waviness is not included. In the present work,  $J$ -integral approach will be used to incorporate the waviness. This will aid in the design and optimization of nacre-like materials. Understanding the relationship between bulk property of materials and micro scale structure and mechanics is an important contribution toward designing bioinspired engineered materials.

### **3.3. Optimization Algorithms**

Bioinspired material design is concerned with extracting the basis and the mechanisms of good design of nature to make advanced synthetic materials. In this process, many efforts have been done in understanding the behavior of biological materials with superior mechanical properties and trying to model their mechanical properties. As well as applying these principles in designing new synthetic materials. Hard biological materials such as nacre has been a source of inspiration. Nacre has a simple structure yet it is optimized for high stiffness, strength and toughness. There are few works related to optimization of nacre. Barthelat [118] has used a weighted sum method to solve the multi-objective optimization considering the objective is to maximize stiffness, strength and toughness. The weighted sum method is mathematically simple since the multi-objective is converted to a single objective problem and yet the users' preferences

for acceptable tradeoffs between desired properties need to be known prior to solving the problem. Another related work is done by Guo and Gao [119] in which Genetic Algorithm was used. The objective is to maximize the stiffness and toughness of the structure considering the design variable to be a unit cell in a representative volume element (RVE). So the problem is to find the optimal distribution of hard mineral and ductile biopolymer in the RVE. Guo combined the two objective functions into one. Thus solving the optimization problem as a single objective optimization problem. It has been shown that the staggered structure of hard biological materials such as nacre and bone are optimized structures for maximum structural support and flaw tolerance. Yourdkhani and his coworkers [72] have formulated an optimization problem considering the overall structure of the shell in which the macro structure of shell as well as the microstructure of nacre are optimized for optimum resistance of perforation by a sharp indenter. Yourdkhani et al. used Nelder-Mead method which is a heuristic numerical method used to find a minimum or maximum of a single objective function in a multidimensional space. Design guideline for synthesis of two-layer shells for protection purposes were proposed. In all of the previous work, all of the objectives are combined in a single objective and the problem is solved as a single objective optimization problem. The main disadvantage is that the user preferences should be known prior to solving the optimization problem and only one solution is obtained. In this work, a multi-objective optimization problem is solved to get a set of optimal solutions in which the designers can select according to their preferences.

#### 4. WAVINESS STIFFNESS MODEL\*

The high stiffness of nacre is attributed to its high mineral content. Of interest, the specific mechanism creating the high toughness of nacre is less obvious although remarkable. Nacre's toughness is explained by the ability of nacre to deform. As nacre deforms past its yield point, it develops large inelastic strain in large volumes around defects and cracks. The failure strain of nacre exceeds 1%. A 1% failure strain rate is 100 times that of typical engineered ceramics. High strain is mainly due to tablet sliding and waviness. The work here builds on the work of Zhu and Barthelat [5] who built a millimeter size wavy poly-methyl-methacrylate (PMMA) sample inspired from the structure of nacre. They developed an analytical model for the synthetic nacre. In their model, they did not account for shear stress between the tablets but instead used coulomb friction. In the present work, the shear stress between the tablets is included. Understanding the relationship between bulk property of materials and micro scale structure and mechanics is an important contribution toward designing bioinspired engineered materials [113].

The structure of nacre and a representative volume element (RVE) are shown in Figures 12a, and 12b. The RVE is symmetric with respect to the horizontal axis and one half of the RVE can be used in order to reduce the computation cost. The reduced RVE is

---

\*Reprinted with permission from, "Modeling of a biological material nacre: Waviness stiffness model," by Authors' N. S. Al-Maskari, D. A. McAdams, and J. N. Reddy, 2017. *Materials Science and Engineering: C*, vol. 70, Part 1, pp. 772-776, Copyright 2016 by Elsevier B.V.

shown in Figure 12c and the applied stress is shown in Figure 12d. The tablet has a length  $L$ , thickness  $t$ , a dovetail angle  $\theta$ , and a modulus of elasticity  $E_t$ . The length where the adjacent tablets from different layers overlap is denoted by  $L_o$ . The interface is of thickness  $h$  and shear modulus  $G_i$ .

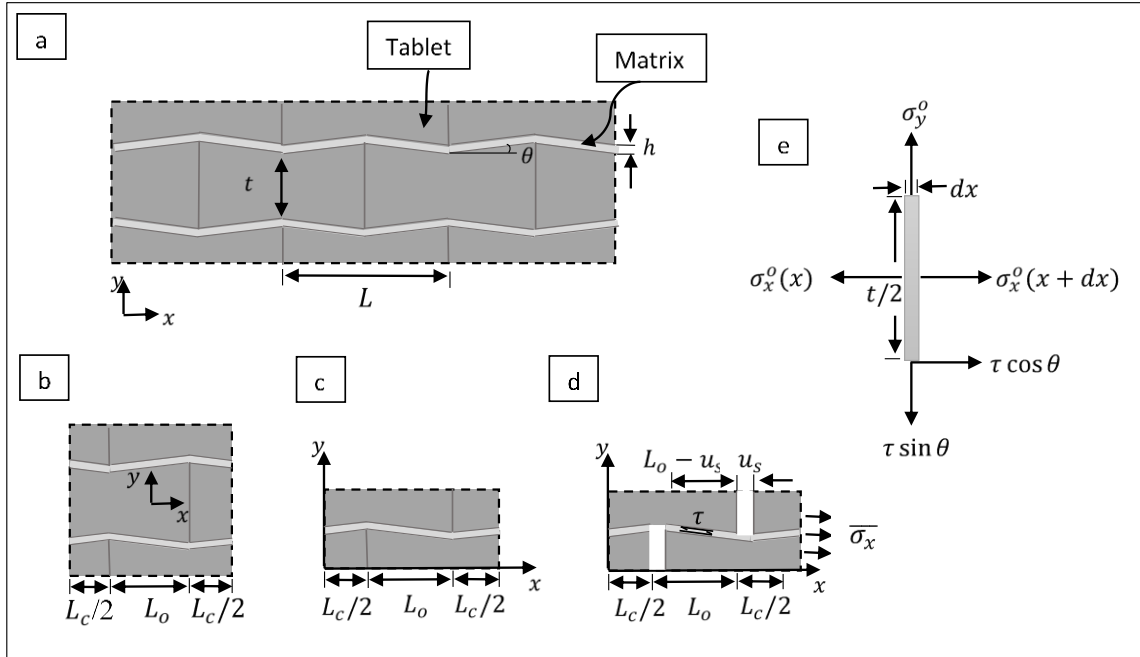


**Figure 12.** a) Structure of nacre; b) RVE symmetric about the x-axis; c) A reduced RVE; d) A reduced RVE when a load is applied; e) Forces in a differential element in the overlap region. Reprinted with permission from [113].

The large extension of the RVE is largely due to tablets sliding, hence the axial strains in the tablets are neglected, and it is given by

$$\bar{\epsilon}_x \approx \frac{u_s}{L_0 + L_c} + \frac{\Delta_t}{L_0 + L_c} \quad (4.1)$$

where  $u_s$  is the sliding distance and  $\Delta_t$  is the extension due to tablet.

Load transfer at the interface is the key mechanism for the composite. Balancing the load of a differential element in the overlap region, as shown in Figure 12e, results in the following stresses

$$\frac{d\sigma_x^o}{dx} = \frac{\tau \cos \theta}{t/2} \quad (4.2)$$

$$\sigma_y^o = \tau \sin \theta \quad (4.3)$$

where  $\sigma_x^o$  and  $\sigma_y^o$  are the axial and transverse stresses in the overlap region, respectively.

Integrating equation (4.2) over  $x$  from 0 to  $L_0 - u_s$  yields

$$\sigma_x^o = \frac{L_0 - u_s}{t/2} \tau \cos \theta \quad (4.4)$$

where  $\tau$  is the shear stress at the interface. The shear stress is assumed to be uniform [120].

The shear stress can be calculated from

$$\tau = G_i \gamma \quad (4.5)$$

where  $\gamma$  denotes the shear strain. The shear strain can be calculated from

$$\gamma \approx \frac{\Delta u_x}{\Delta y} + \frac{\Delta u_y}{\Delta x} \approx \frac{u_s}{h} + \tan \theta \quad (4.6)$$

Substituting equation (4.6) into equation (4.5) results in

$$\tau \approx G_i \left( \frac{u_s}{h} + \tan \theta \right) \quad (4.7)$$

Substitution of equation (4.7) into equations (4.3) and (4.4) yields

$$\sigma_x^o = 2G_i \frac{(L_0 - u_s)}{t} \left( \frac{u_s}{h} + \tan \theta \right) \cos \theta \quad (4.8)$$

$$\sigma_y^o = G_i \left( \frac{u_s}{h} + \tan \theta \right) \sin \theta \quad (4.9)$$

The applied axial stress is given by

$$\bar{\sigma}_x = \sigma_x^c \quad (4.10)$$

The axial stress is transmitted in the core region through a thickness  $t + h$  and in the overlap region through  $(t + h)/2$  thus  $\sigma_x^0$  and  $\sigma_x^c$  are related via

$$\sigma_x^0 = 2\sigma_x^c \quad (4.11)$$

The transverse stresses in the core and overlap region can be related from a force balance in the y-axis via

$$(L_0 - u_s)\sigma_y^0 + L_c\sigma_y^c = 0 \quad (4.12)$$

Combining equations (4.8), (4.10), and (4.11) the axial stress is obtained as

$$\bar{\sigma}_x = G_i \frac{L_0 - u_s}{t} \left( \frac{u_s}{h} + \tan \theta \right) \cos \theta \quad (4.13)$$

The extension due to tablet is given by

$$\Delta_t = \frac{\sigma_x^c}{E_t} L_c \quad (4.14)$$

Combining equations (4.1), (4.13) and (4.14) results in

$$\begin{aligned} \bar{\sigma}_x = \frac{G_i \cos \theta}{th} & \left[ L_0 h \tan \theta + \bar{\varepsilon}_x (L_0 + L_c) (L_0 \right. \\ & \left. - h \tan \theta) \frac{E_t h t}{E_t h t + L_c G_i (L_0 - h \theta)} \right. \\ & \left. - \bar{\varepsilon}_x^2 (L_0 + L_c)^2 \left( \frac{E_t h t}{E_t h t + L_c G_i (L_0 - h \theta)} \right)^2 \right] \end{aligned} \quad (4.15)$$

The stress strain curve can be plotted and fitted linearly in the elastic region to determine the elastic modulus from the fitting equation. Note that because of the nonlinear relation between the stress ( $\bar{\sigma}_x$ ) and strain ( $\bar{\varepsilon}_x$ ), it is not possible to express the elastic modulus explicitly. Equation (4.15) shows that there exists a geometric strain hardening

indicating spreading of nonlinear deformation thus maximizing energy dissipation and in turn maximizing toughness. Note that the transvers stresses in the overlap and core region can be obtained using equations (4.9) and (4.12). The shear stress at the interface can be calculated from equations (4.7) and (4.1).

The model developed in this section represents a more accurate geometry and loading conditions of nacre. The stiffness of nacre can be obtained from the stress-strain relationship as seen in equation 4.14. Considering waviness is crucial in obtaining accurate estimation of stiffness. In addition, evaluating transverse stresses may be needed depending on the application [113].

#### **4.1. Results and Discussions**

Data for nacre and a borosilicate glass with polyurethane taken from literature were used to validate the model developed above. For nacre, the tablet's length is approximately  $5\mu\text{m}$ , its thickness is approximately  $5\mu\text{m}$ , the dovetail angle is  $5^\circ$  and the Elastic Modulus of a single tablet along the plane of the tablet is 100 GPa [1]. The thickness of the matrix is 28 nm and has a shear modulus of 1.4 GPa [1]. The overlap region was considered to be half the length of the tablet. The borosilicate glass with polyurethane was made with a laser engraving technique by carving weak interfaces within a brittle material. More details about the laser engraving technique are found in reference [10]. The modulus of elasticity was calculated for the case of flat surface ( $\theta = 0^\circ$ ) which is equivalent with earlier models and for the case of a dovetail angle of  $5^\circ$  which represents the waviness in nacre. The results are compared with experimentally measured moduli taken from literature [1, 4, 41] and are shown in Table 4.

**Table 4** Comparison of elastic moduli

<b>Elastic Moduli</b>	<b>Flat surface (no waviness)</b>	<b>Wavy surface with <math>\theta = 5^\circ</math></b>	<b>Experimentally measured</b>
<b>nacre</b>	79 GPa	65 GPa	69 GPa
<b>borosilicate glass with polyurethane</b>	0.46 GPa	0.61 GPa	0.667 GPa

Table 4 shows that the elastic modulus for nacre for the case of wavy surface with a dovetail angle of  $5^\circ$  is within the experimentally measured modulus found in literature and has a better prediction compared to nacre with flat surface which is used in earlier models. In addition, for the case of borosilicate glass with polyurethane, the elastic modulus for the case of a wavy surface has a value closer to the experimentally measured value than that of a flat surface. This is expected since the geometrical representation of the wavy surface resembles that of the actual nacre more than the flat surface. This result also confirms that when designing and realizing an engineered nacre like material, waviness must be considered as one of the design variables. It may be noted that the elastic modulus obtained is less than the elastic modulus of the individual tablet because the structure sacrifices some stiffness to increase the toughness [113].

#### **4.2. Dovetail Angle**

Having a way to predict the dovetail angle is desired to better design a nacre like material. Since the waviness in the tablet is one of the reasons for having a remarkable

combination of stiffness and toughness. Thus looking at equation (4.7) and solving for the dovetail angle results in

$$\theta = \frac{\tau}{G_i} - \frac{u_s}{h} \quad (4.16)$$

where the value of the sliding distance can be obtained from equation (4.1) ignoring the second term and substituted in equation (4.16), resulting in

$$\theta = \frac{\tau}{G_i} - \frac{\varepsilon_x(L_c + L_0)}{h} \quad (4.17)$$

Equation (4.17) indicates that the angle depends on the interface properties; shear modulus, interface thickness, and shear stress as well as the axial strain and the thickness of the tablets. In order to calculate the dovetail angle for a synthetic material, the shear strength ( $\tau_s$ ) and the maximum elastic axial strain are used as directed below

$$\theta = \frac{\tau_s}{G_i} - \frac{\varepsilon_{x,elastic}(L_c + L_0)}{h} \quad (4.18)$$

This equation shows that the angle depends on the ratio between interface strength and interface modulus as well as the ratio  $(L_c + L_0)/h$  and elastic axial strain.

Testing the equation with nacre and the borosilicate glass with polyurethane, it was found that the dovetail angles are  $4.8^\circ \sim 5^\circ$  for nacre and  $3.15^\circ$  for borosilicate glass with polyurethane. In the literature, the dovetail angle for nacre is very small and less than  $5^\circ$  [4, 5]. For borosilicate glass with polyurethane, angles greater than  $5^\circ$  cause tablets fracture and it is desired to have angles less than  $5^\circ$ . This indicates that dovetail angle of  $3.15^\circ$  is ideal for the case of borosilicate glass with polyurethane [113].

## 5. WAVINESS TOUGHNESS MODEL

Hard biological materials such as nacre, bone and teeth exhibit high values of toughness although it is mainly made of a ceramic material. Ceramic materials are brittle and fail in a catastrophic manner hence they have low values of toughness. The waviness toughness model concerns with mode I crack. Fracture toughness is quantified using the  $J$ -integral. The toughening mechanisms considered are bridging toughening ( $J_B$ ) and process zone toughening ( $J_P$ ) and are shown in Figure 13. Initially, toughness is quantified where it is assumed that fully developed wake is present. Then, the R-curve of nacre and nacre-like materials is obtained assuming the wake is developing with crack extension.

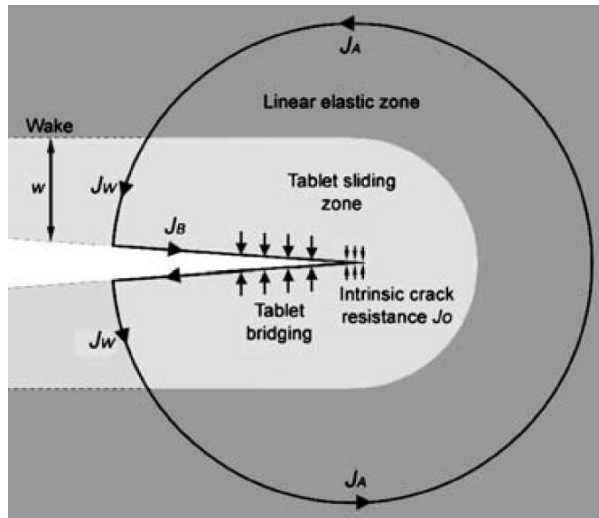


**Figure 13.** Schematic showing a crack in nacre with J-integral contours. Reprinted with permission from [79]

### 5.1. Quantifying Toughness

The net toughness,  $J_T$  can be giving by

$$J_T = J_B + J_P \quad (5.1)$$

where  $J_B$  is the contribution from bridging toughening and  $J_P$  is the contribution from process zone toughening.

The definition of the  $J$ -integral is given by equation (5.2).

$$J = \int_{\Gamma} \omega dy - \mathbf{T}_i \frac{d\mathbf{u}}{dx} ds \quad (5.2)$$

where  $\Gamma$  is an arbitrary path clockwise around the apex of the crack,  $\mathbf{T}_i$  are traction components,  $\mathbf{u}_i$  are the displacement components,  $ds$  is the incremental length along the path and  $\omega$  is the strain energy and is giving by

$$\omega = \int_0^{\varepsilon_{ij}} \sigma_{ij} d\varepsilon_{ij} \quad (5.3)$$

The first term in the definition of the  $J$ -integral, in equation (5.2), represents the strain energy release rate that can be calculated using equation (5.3). The second term is the work (energy) per unit fracture surface area, in a material and can be computed using equations

$$\mathbf{T}_i = T_x i + T_y j \quad (5.4)$$

$$\mathbf{T}_i = (\sigma_{xx} n_x + \sigma_{xy} n_y) i + (\sigma_{xy} n_x + \sigma_{yy} n_y) j \quad (5.5)$$

$$\frac{d\mathbf{u}}{dx} = \frac{du}{dx} i + \frac{dv}{dx} j \quad (5.6)$$

where  $\sigma_{xx}$  is the stress in  $x$ -axis,  $\sigma_{xy}$  is the shear stress,  $\sigma_{yy}$  is the stress in  $y$ -axis and  $n_i$  is the normal vector.

In bridging toughening, the tablets provide tractions across the crack wake. Thus the crack tip is shielded from the applied load. Applying the definition of the  $J$ -integral combined with equations (5.4) and (5.6) results in

$$J_B = \int_{\Gamma} \mathbf{T}_i \frac{d\mathbf{u}}{d\mathbf{x}} ds = \int_{\Gamma} \left( T_x \frac{du}{dx} + T_y \frac{dv}{dx} \right) ds \quad (5.7)$$

The tractions, in the  $x$ -axis, on one tablet cancel each other because of the dovetail feature. Thus only tractions along  $y$ -axis exists and is given by

$$T_y = \frac{\tau_s L \cos \theta}{2t} \quad (5.8)$$

Substituting  $T_y$  in equation (5.7) yields

$$J_B = 2 \int_0^{u_{max}/2} \frac{\tau_s L \cos \theta}{2t} du \quad (5.9)$$

Integrating equation (5.9) results in

$$J_B = \frac{1}{2} \frac{L}{t} \tau_s u_{max} \cos \theta \quad (5.10)$$

This bridging toughening occurs over a length called bridging or cohesive length ( $\lambda$ ) and is given by [23]

$$\lambda = \frac{\pi J_B E}{8 \sigma_s^2} \quad (5.11)$$

The process zone toughening includes micro-crack toughening and operates in materials exhibiting inelasticity (i.e. irreversible residual strain) after unloading. The stress concentration at the crack front creates a local inelastic deformation zone termed a process zone experiences hysteretic unloading in the wake of the tip, resulting in higher toughness.

Using the definition of the  $J$ -integral, the process zone toughness can be quantified as follows

$$J_P = 2 \int_0^w \int_0^{\varepsilon_{ij}} (\sigma_x d\varepsilon_x + \sigma_y d\varepsilon_y) dy \quad (5.12)$$

where  $w$  is the width of process zone.

The stresses are obtained from the waviness stiffness model (discussed in section 4) as shown in equations (5.13) and (5.14)

$$\sigma_x = \frac{u_s - L_o}{L_c} \tau_s \sin \theta \quad (5.13)$$

$$\sigma_y = \frac{L_o - u_s}{t} \tau_s \cos \theta \quad (5.14)$$

Substituting equations (5.13) and (5.14) into equation (5.12) results in

$$J_P = 2 \int_0^w \left[ \int_0^{\varepsilon_x} \frac{u_s - L_o}{L_c} \tau_s \sin \theta d\varepsilon_x + \int_0^{\varepsilon_y} \tau_s \cos \theta \frac{L_o - u_s}{t} d\varepsilon_y \right] dy \quad (5.15)$$

Integrating the inner bracket in equation (5.15) yields

$$J_P = 2 \int_0^w \left[ \frac{u_s - L_o}{L_c} \tau_s \sin \theta \varepsilon_{x,r} + \tau_s \cos \theta \frac{L_o - u_s}{t} \varepsilon_{y,r} \right] dy \quad (5.16)$$

where  $\varepsilon_{x,r}$  and  $\varepsilon_{y,r}$  are the residual strains away from the crack tip; along and across the crack, respectively. The residual strains are zero on the boundary of the wake and have a maximum value at the crack face thus they are assumed to be linear as follows

$$\varepsilon_{x,r} = \left( \varepsilon_{x,max} - \frac{\sigma_x}{E} \right) \left( 1 - \frac{y}{w} \right) \quad (5.17)$$

$$\varepsilon_{y,r} = \left( \varepsilon_{y,max} - \frac{\sigma_y}{E} \right) \left( 1 - \frac{y}{w} \right) \quad (5.18)$$

Substituting equations (5.17) and (5.18) into equation (5.16) and performing the integration yields

$$J_P = w \left[ \frac{u_s - L_o}{L_c} \tau_s \sin \theta \left( \varepsilon_{x,max} - \frac{\sigma_x}{E} \right) + \tau_s \cos \theta \frac{L_o - u_s}{t} \left( \varepsilon_{y,max} - \frac{\sigma_y}{E} \right) \right] \quad (5.19)$$

The net toughness is calculated by substituting equations (5.10) and (5.19) into (5.1)

$$J_T = w \left[ \frac{u_s - L_o}{L_c} \tau_s \sin \theta \left( \varepsilon_{x,max} - \frac{\sigma_x}{E} \right) + \tau_s \cos \theta \frac{L_o - u_s}{t} \left( \varepsilon_{y,max} - \frac{\sigma_y}{E} \right) \right] \quad (5.20)$$

$$+ 0.5 \frac{L}{t} \tau_s u_{max} \cos \theta$$

The width of the process zone can be computed as follows [121]

$$w = \frac{J_T E}{4\sigma_s^2} \quad (5.21)$$

where  $\sigma_s$  is the strength of the composite and is giving by

$$\sigma_s = \frac{L_o}{t + h} \tau_s \quad (5.22)$$

Substituting equations (5.22) into (5.21) and combining with equation (5.20) yields

$$J_T = \frac{0.5 \tau_s u_{max} \cos \theta L/t}{1 - \frac{E \tau_s}{4\sigma_s^2} \left[ \frac{u_s - L_o}{L_c} \left( \varepsilon_{x,max} - \frac{\sigma_x}{E} \right) \sin \theta + \frac{L_o - u_s}{t} \left( \varepsilon_{y,max} - \frac{\sigma_y}{E} \right) \cos \theta \right]} \quad (5.23)$$

where the maximum strains  $\varepsilon_{x,max}$  and  $\varepsilon_{y,max}$  are giving below

$$\varepsilon_{x,max} = \frac{L_o \theta}{h + t} \quad (5.24)$$

$$\varepsilon_{y,max} = \frac{u_{max}}{L} \quad (5.25)$$

Thus substituting equations (5.24) and (5.25) into equation (5.23), the toughness of nacre considering bridging and process zone toughening mechanism will be given by

$$J_T = \frac{0.5\tau_s u_{max} \cos \theta L/t}{1 - \frac{E\tau_s}{4\sigma_s^2} \left[ \frac{u_s - L_o}{L_c} \left( \frac{L_o\theta}{h+t} - \frac{\sigma_x}{E} \right) \sin \theta + \frac{L_o - u_s}{t} \left( \frac{u_{max}}{L} - \frac{\sigma_y}{E} \right) \cos \theta \right]} \quad (5.26)$$

## 5.2. Crack Resistance Curve (R-curve)

In obtaining the R-curve, the shape of frontal zone is assumed to be circular and the width of the process zone is increased with crack extension. This regime is called non-steady regime in which the toughness is increased with crack extension. In this case, the strain energy is given by equation (5.3) to be

$$\omega = \int_0^{\varepsilon_{ij}} (\sigma_x d\varepsilon_x + \sigma_y d\varepsilon_y) dy \quad (5.27)$$

Performing the integration results in

$$\omega = \sigma_x \varepsilon_{x,r} + \sigma_y \varepsilon_{y,r} \quad (5.28)$$

Substituting equations (5.16) and (5.17) into equation (5.28) yields

$$\omega = \left[ \sigma_x \left( \varepsilon_{x,max} - \frac{\sigma_x}{E} \right) + \sigma_y \left( \varepsilon_{y,max} - \frac{\sigma_y}{E} \right) \right] \left( 1 - \frac{y}{w} \right) \quad (5.29)$$

Applying the definition of  $J$ -integral, equation (25.), the toughness due to process zone is given by

$$J_P = \iint_{dW} \omega dy dx \quad (5.30)$$

Substituting equation (5.29) into equation (5.30) results in

$$J_P = \iint_{dW} \left[ \sigma_x \left( \varepsilon_{x,max} - \frac{\sigma_x}{E} \right) + \sigma_y \left( \varepsilon_{y,max} - \frac{\sigma_y}{E} \right) \right] \left( 1 - \frac{y}{w} \right) dydx \quad (5.31)$$

Excluding from integration the terms that does not depends on  $x$  and  $y$  yields

$$J_P = \left[ \sigma_x \left( \varepsilon_{x,max} - \frac{\sigma_x}{E} \right) + \sigma_y \left( \varepsilon_{y,max} - \frac{\sigma_y}{E} \right) \right] \iint_{dW} \left( 1 - \frac{y}{w} \right) dydx \quad (5.32)$$

The integration is solved and is given by [23]

$$\iint_{dW} \left( 1 - \frac{y}{w} \right) dydx = wF\left(\frac{dw}{da}\right) \quad (5.33)$$

where  $F\left(\frac{dw}{da}\right) = F(n)$  and is given by [122]

$$F(n) = \left( 2 \frac{(1+n)\sqrt{1+2n}}{n} - ncot^{-1}\left(\frac{n}{\sqrt{1+2n}}\right) - \frac{(1+2n)^{3/2}}{n^2} \ln\left(\frac{1+2n}{1+n}\right) \right) \quad (5.34)$$

Details of how equation (5.34) is obtained can be found in [122]. Substituting equations (5.34) and (5.33) into equation (5.32) yields

$$J_P = \left[ \sigma_x \left( \varepsilon_{x,max} - \frac{\sigma_x}{E} \right) + \sigma_y \left( \varepsilon_{y,max} - \frac{\sigma_y}{E} \right) \right] wF\left(\frac{dw}{da}\right) \quad (5.35)$$

Equation (5.35) express the toughness due to process zone. The toughness due to bridging will not be constant. The toughness will increase as the cohesive length is increased during crack extension. This increase is linear since the closure stress applied over the cohesive length is uniform. Hence, the bridging toughness is given by

$$J_B = \begin{cases} \left(\frac{a}{\lambda}\right) \frac{1}{2} \frac{L}{t} \tau_s u_{max} \cos \theta & 0 \leq a \leq \lambda \\ \frac{1}{2} \frac{L}{t} \tau_s u_{max} \cos \theta & a > \lambda \end{cases} \quad (5.36)$$

The net toughness due to bridging and process zone can be given by

$$J_T = J_B + \left[ \sigma_x \left( \varepsilon_{x,max} - \frac{\sigma_x}{E} \right) + \sigma_y \left( \varepsilon_{y,max} - \frac{\sigma_y}{E} \right) \right] wF \left( \frac{dw}{da} \right) \quad (5.37)$$

Substituting equations (5.24) and (5.25) into equation (5.37) yields

$$J_T = J_B + \left[ \sigma_x \left( \frac{L_o \theta}{h + t} - \frac{\sigma_x}{E} \right) + \sigma_y \left( \frac{u_{max}}{L} - \frac{\sigma_y}{E} \right) \right] wF \left( \frac{dw}{da} \right) \quad (5.38)$$

Equation 37 is a first order differential equation which can be solved by MATLAB in order to plot the R-curve. The calculated R-curve for nacre is plotted in the following section. Sample code is shown in Appendix A.

### 5.3. Results and Discussions

First the model is validated with existing data of nacre from red abalone shell available in the literature. The tablets are considered to be made of aragonite and the interface is made of biopolymer similar to that of nacre. Barthelat and Espinosa [79] have established the crack resistance curve for nacre as shown in Figure 14. A sample of nacre was tested and the elastic modulus was found to be ~80 GPa, strength of 70 MPa and strain to failure of 0.15. The bridging toughening was estimated to be 0.012 and the intrinsic toughness is about 0.3 kJ/m<sup>2</sup>. Using this as input to our code, the differential equation (5.38) was solved analytically via MATLAB and the resulted R-curve is shown in Figure 15.

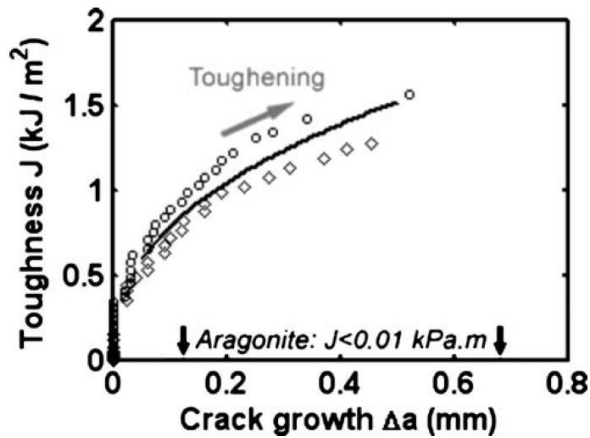


**Figure 14.** R-curve for nacre (for two experiments) with logarithmic fit. Reprinted with permission from [79]

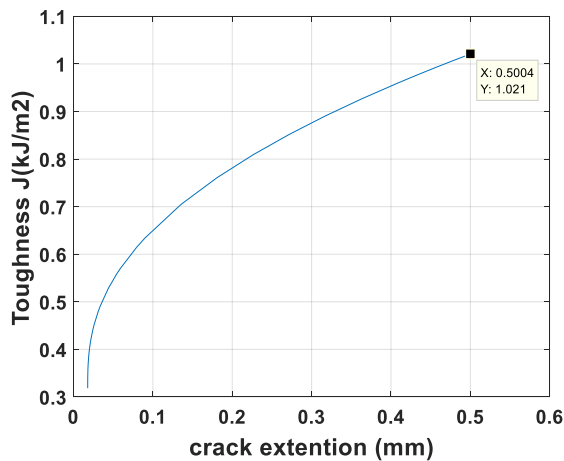


**Figure 15.** R-curve obtained from waviness toughness model

Note that the maximum value obtained experimentally in which the  $J$ -integral continues to characterize the state of stress at the crack tip is 1.25 kJ/m<sup>2</sup> and 1.5 kJ/m<sup>2</sup> for the two experiments. The maximum value obtained by our model is 1.021 kJ/m<sup>2</sup> it is slightly lower than the value obtained experimentally. This may be because of other toughening mechanisms that are not considered such as crack deflection. However, the

resulted R-curve is in good agreement with the actual R-curve for nacre. This validates the model specifically the  $J$ -integral value of the process zone since the bridging contribution and the intrinsic toughness were input to the model. The bridging contribution to toughness ( $J_b$ ) cannot be verified since the aspect ratio of the tablet and the maximum displacement was not stated in the article. However, the upper and the lower bound of the bridging toughness ( $J_b$ ) can be computed via equation (10). Considering tablet's length of 5-10  $\mu\text{m}$ , tablet's thickness of 0.4-0.5  $\mu\text{m}$ , maximum strain of 0.015 and shear strength of the interface between 25-37MPa. The bridging contribution to toughness is between 0.0094-0.0694  $\text{kJ/m}^2$ . The bridging toughness was quantified in the literature to be 0.012  $\text{kJ/m}^2$  [79] which is within the estimated bridging toughness just obtained from our model.

Second, the waviness toughness model is validated with another available experimental data for nacre as well as with the model developed by Barthelat and Rabiei [23]. Rabiei et al. [86] have obtained R-curve for red abalone as shown in Figure 16. The lower bound corresponds to an elastic modulus of 70 GPa, Strength of 100 MPa and max axial strain of 0.008. The upper bound corresponds to an elastic modulus of 80 MPa, data for nacre for red abalone. The tablet's properties are; elastic modulus is 100 GPa, length is 5-10  $\mu\text{m}$ , thickness is 0.4-0.5  $\mu\text{m}$  and dovetail angle  $1^\circ$  - $5^\circ$ . The overlap length is 0.1-0.5 of tablets length. The interface properties are; shear modulus is 1.4 GPa, shear strength is 25-37 MPa and thickness of 20-30 nm. In our model the lower bound corresponds to elastic modulus of 36.48GPa, Strength of 23.58 MPa and max axial strain of 0.008. The upper bound corresponds to elastic modulus of 95 GPa, strength of 440 MPa and max axial strain of 0.015. The upper and lower bound of our model combined with

experimental data of Figure 14 and 16 is shown in Figure 17. Note that the developed model in this article, bounds all the experimental data. Whereas the earlier developed model bounds only the experimental R-curve obtained by Rabiei et al. [86] This may be attributed to difference elastic modulus, strength and toughness used as upper and lower bound. The toughness value of the upper bound of our model is about  $2.45 \text{ kJ/m}^2$  this may indicate that actual nacre's toughness can't exceed  $2.45 \text{ kJ/m}^2$ . Nevertheless, extreme cases are considered in our model which help looking at the span of ranges that can be obtained from the model.

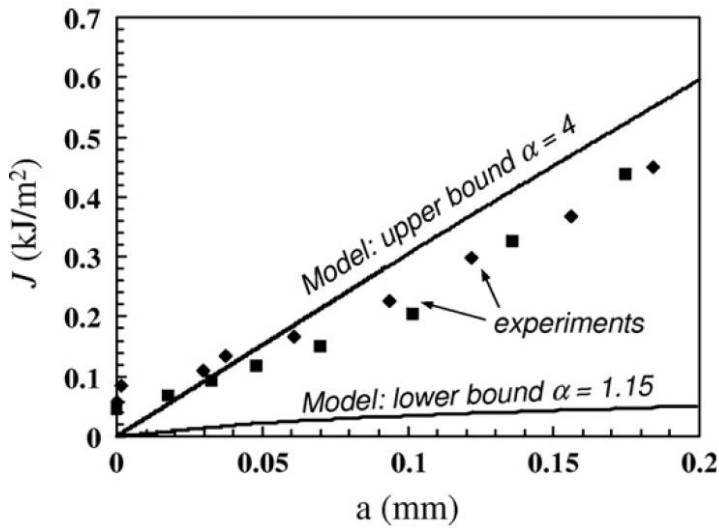


**Figure 16.** R-curve for nacre (for two experiments). Reprinted with permission from [23]

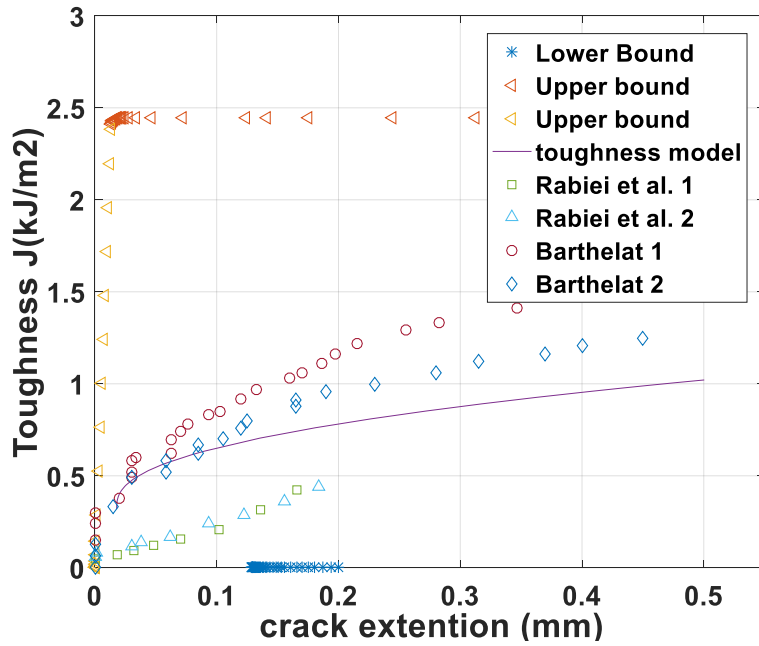


**Figure 17.** R-curve for nacre (for four experiments) and our model

After validating the model, the R-curve of a nacre-like material made of Alumina and poly-methyl-methacrylate ( $\text{Al}_2\text{O}_3/\text{PMMA}$ ) is obtained as shown in Figure 18. The nacre-like material ( $\text{Al}_2\text{O}_3/\text{PMMA}$ ) is synthesized using ice-templated technique [11]. The maximum toughness value obtained at crack extension of 1 mm was  $8 \text{ kJ/m}^2$  while our model predicts a value of  $7.36 \text{ kJ/m}^2$ . As expected, the value is lower than the measured due to unaccounted toughening mechanisms such as crack deflection.

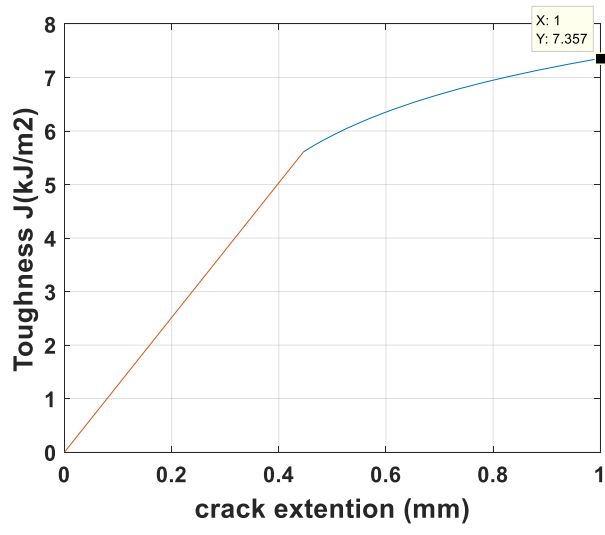


**Figure 18.** R-curve for waviness model for the nacre-like material of Al<sub>2</sub>O<sub>3</sub>/PMMA

## 6. OPTIMIZATION OF NACRE-LIKE MATERIALS

The staggered structure of nacre is composed of tablets embedded into a matrix. In order to capture the mechanics of the staggered structure a representative volume element (RVE) is used. In this work two RVEs are used. The first one is for the case of flat tablets as shown in Figure 19.a and the second one is for the case of wavy tablets as shown in Figure 19.b.

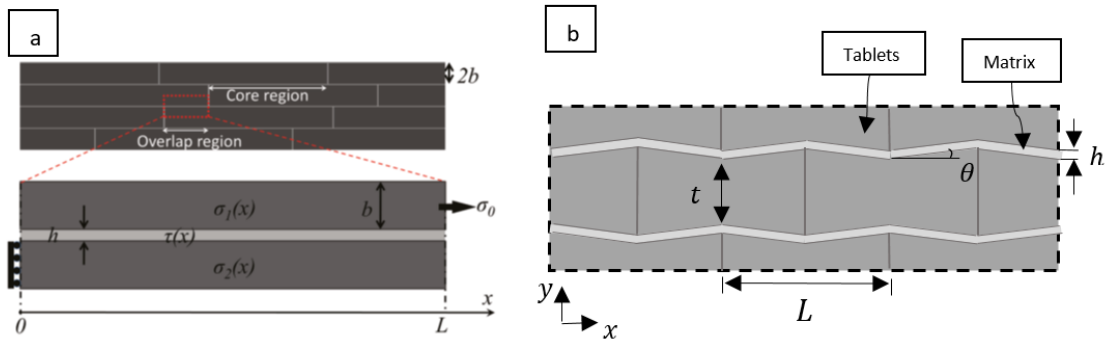


**Figure 19.** Flat and wavy tablets

The wavy configuration is close to the actual nacre's configuration and results in high energy dissipation during deformation which means high toughness. The flat tablet is a simplified configuration that is commonly found in nacre-like materials. The tablet has a length  $L$ , a thickness  $t$ , a dovetail angle  $\theta$ , and a modulus of elasticity  $E_t$ . The length where the adjacent tablets from different layer overlap is denoted by  $L_o$ . The interface (which is the matrix) is of thickness  $h$  and shear modulus  $G_i$ . Three mechanical properties

namely stiffness, strength and toughness will be discussed briefly in the following subsections.

## 6.1. Objective Functions

The three objective functions considered are discussed below.

### 6.1.1. Stiffness

The elastic modulus (stiffness) of staggered structure for the case of flat tablets is given by equation (6.1). This equation was developed by Kotha [82] for flat tablets considering only stresses along the tablets and neglecting transverse stresses

$$\frac{1}{E} = \left(1 + \frac{h}{t}\right) \left(\frac{1}{E_t} + 2th\gamma \left(\frac{1 + \cosh(\gamma L)}{LG_i \sinh(\gamma L)}\right)\right) \quad (6.1)$$

where

$$\gamma = \sqrt{\frac{G_i}{E_t th}} \quad (6.2)$$

While the elastic modulus for the case of wavy tablets is obtained by linearizing equation (4.15)

$$E = \frac{t}{2t + h} \frac{E_t ht}{E_t ht + L_c G_i (L_0 - h\theta)} \frac{G_i}{th} L(L_0 - h\theta) \quad (6.3)$$

### 6.1.2. Strength

Failure of the nacreous layer may be due to tablets fracture when the ultimate tensile strength of the tablets is reached or it may be due to failure of the interface when the shear strength of the interface is reached. It is assumed in the work presented here that failure occurs at the interface to allow tablet sliding and energy dissipation through inelastic deformation at the interface. The shear strength of the interface is constant

assuming the interface is perfectly plastic and fully yielded. Hence the force carried by the tablets is  $L_0\tau_s$  where  $\tau_s$  is the shear strength of the interface. Neglecting the tensile stress carried by the interface, the strength of the RVE,  $\sigma_s$ , can be calculated as [118]

$$\sigma_s = \frac{L_0}{t+h}\tau_s \quad (6.4)$$

where  $L_0$  is the overlap length,  $t$  is the thickness of the tablet and  $h$  is the thickness of the interface. This strength model is valid for flat tablets as well as wavy tablets [123].

### 6.1.3. Toughness

The toughness of staggered structure, denoted by  $J$ , for the case of flat tablets is given by equation (6.5). This comes from bridging toughening and process zone toughening mechanisms. More details is found in reference [23]

$$J = \frac{\tau_s u_{max} L/t}{2.5 - \frac{E u_{max} t}{\tau_s L^2}} \quad (6.5)$$

While the toughness for the case of wavy tablets is given by equation (6). Considering the same toughening mechanisms and including the stresses in the transverse direction. Detailed derivation is found in section 5.

$$J \quad (6.6)$$

$$= \frac{0.5\tau_s u_{max} L/t}{1 - \frac{E\tau_s}{4\sigma_s^2} \left[ \frac{u_s - L_0}{L_c} \left( \frac{L_0\theta}{h+t} - \frac{\tau_s(u_s - L_0)}{EL_c} \right) \theta + \frac{L_0 - u_s}{t} \left( \frac{u_{max}}{L} - \frac{\tau_s(L_0 - u_s)}{tE} \right) \right]}$$

where  $L$  is tablet's length,  $t$  is tablet's thickness,  $L_0$  is the overlap length  $L_c$  is core length given by  $L_c = L - L_0$ ,  $\theta$  is dovetail angle,  $G_i$  is shear modulus of the interface,  $h$  is the thickness of the interface,  $\tau_s$  is the shear strength of the interface,  $u_s$  is the sliding distance,

$u_{max}$  is the maximum sliding distance,  $\sigma_s$  is the strength of RVE and  $E$  is the elastic modulus of the RVE.

## 6.2. Formulation and Solution Approach

Natural nacre has a desirable property mix of strength, stiffness, and toughness. Thus, we wish to have an engineered nacre with the best strength, stiffness, and toughness we can achieve. Stating this more formally, the objective function is to maximize stiffness ( $E$ ), strength ( $\sigma_s$ ) and toughness ( $J$ ) subjected to some constraints for tablets with flat and wavy surfaces as will be explained shortly. The design variables are tablet's length ( $L$ ), tablet's thickness ( $t$ ), interface thickness ( $h$ ) and overlap length ( $L_o$ ) for the case of tablets with flat surface and the dovetail angle ( $\theta$ ) is added for the case of tablets with wavy surface.

Before exploring the optimization problem, some constraints were set up to stay within the bounds of our model and the physics of the bulk material. Additionally, other constraints were added to simplify the problem such that the optimization algorithm will converge in a practical time frame. The constraints are discussed below.

### 6.2.1. Constraints

For the toughening mechanisms to operate the tablets should slide on each other upon load application and the individual tablets should not break. To avoid the fracture of an individual tablets Bekah et al. [123] assumed an edge crack extending halfway through the tablet and suggested that the stress intensity factor  $K_I$  should be less than the fracture toughness of individual tablet  $K_{IC}$ . Where  $K_I$  is given by

$$K_I = 2.83 \sigma_s \sqrt{\pi t / 2} \quad (6.7)$$

Combining equation (6.4) and (6.7) and writing the condition  $K_I < K_{IC}$ . The constraint for preventing tablet fracture is given by

$$\frac{L}{t} < 0.56 \frac{K_{IC}}{\tau_s \sqrt{t}} \quad (6.8)$$

The strength of the composite, as equation (6.4) suggested, is not guaranteed to be higher than the strength of the interface. Assuming the interface is ductile and behaves as linear elastic-perfectly plastic, the interface is governed by Von Mises plasticity. The shear strength of the interface is related to its strength by

$$\sigma_s = \sqrt{3} \tau_i \quad (6.9)$$

Comparing equation (6.4) and (6.9), the strength of the composite will be higher than the interface if [118]

$$\frac{L_0}{t + h} > \sqrt{3} \quad (6.10)$$

There are some variations in overlap lengths found in actual biological and engineering structures. In order to examine trends, the following relation will be considered:

$$0 < \frac{L_0}{L} \leq 0.5 \quad (6.11)$$

In order to ensure the structure is like brick and mortar structure, the following conditions should be met

$$L \geq t \quad (6.12)$$

$$t \geq h \quad (6.13)$$

An additional constraint for the case of tablets with wavy surface considering the material of the composite is that of the actual nacre in order to resemble actual nacre which is given by:

$$\theta < 5^\circ \quad (6.14)$$

### 6.2.2. Multi-Objective Formulation

A multi-objective optimization solution search is explored for several cases as shown in Table 1. The first three cases allow us to validate the accuracy of our model and compare its output to known data for existing nacre and bioinspired nacre. In the fourth case the material properties are incorporated in the optimization algorithm. Hence the best combination of material and geometrical structure is obtained. The material is limited to ceramic/polymer composite since the toughness model developed assumes the tablets are made of ceramic materials.

**Table 5** Solution approach cases

	<b>Tablet Type</b>	<b>Material</b>	<b>Equations for Elastic Modulus and Toughness</b>	<b>Design Variables</b>
<b>Case I</b>	Flat	Nacre	6.1 & 6.5	$(L, t, L_o \& h)$
<b>Case II</b>	Wavy	Nacre	6.3 & 6.6	$(L, t, \theta, L_o \& h)$
<b>Case III</b>	Wavy	Nacre-like Material	6.3 & 6.6	$(L, t, \theta, L_o \& h)$
<b>Case IV</b>	Wavy	Ceramic/Polymer	6.3 & 6.6	$(L, t, \theta, L_o, h, \tau_s, G_i \& E_t)$

Case I represents an RVE with flat tablets considering the constitute materials in the composite are those of natural nacre. That is the tablets are made of calcium carbonate and the interface is made of a biopolymer material. The formulation is as below.

Maximize:

$$E; \frac{1}{E} = \left(1 + \frac{h}{t}\right) \left(\frac{1}{E_t} + 2th\sqrt{G_i/E_t} \left(\frac{1 + \cosh(L\sqrt{G_i/E_t}th)}{LG_i \sinh(L\sqrt{G_i/E_t}th)}\right)\right)$$

$$\sigma_s = \frac{L_0}{t+h} \tau_s$$

$$J = \frac{\tau_s u_{max} L/t}{2.5 - \frac{E u_{max} t}{\tau_s L^2}}$$

Subjected to

$$\frac{L}{t} < 0.56 \frac{K_{IC}}{\tau_s \sqrt{t}}$$

$$\frac{L_0}{t+h} > \sqrt{3}$$

$$0 < \frac{L_0}{L} \leq 0.5$$

$$L > t$$

$$t \geq h$$

Case II is for wavy tablets using actual nacre's calcium carbonate and biopolymer material data. Case II models natural nacre in terms of an improved structure representation and constitute material properties based on measured data. The formulation is shown as follows

Maximize:

$$E = \frac{t}{2t + h} \frac{E_t h t}{E_t h t + L_c G_i (L_0 - h\theta)} \frac{G_i}{t h} L (L_0 - h\theta)$$

$$\sigma_s = \frac{L_0}{t + h} \tau_s$$

$$J = \frac{0.5 \tau_s u_{max} L/t}{1 - \frac{E \tau_s}{4 \sigma_s^2} \left[ \frac{u_s - L_0}{L_c} \left( \frac{L_0 \theta}{h + t} - \frac{\tau_s (u_s - L_0)}{E L_c} \right) \theta + \frac{L_0 - u_s}{t} \left( \frac{u_{max}}{L} - \frac{\tau_s (L_0 - u_s)}{t E} \right) \right]}$$

Subjected to

$$\frac{L}{t} < 0.56 \frac{K_{IC}}{\tau_s \sqrt{t}}$$

$$\frac{L_0}{t + h} > \sqrt{3}$$

$$\theta < 5^\circ$$

$$0 < \frac{L_0}{L} \leq 0.5$$

$$L \geq t$$

$$t \geq h$$

Case III represents an RVE with wavy tablets and using a nacre-like material which is composed of borosilicate glass with polyurethane [10]. The manufacturing method is called laser engraving technique in which weak interfaces are carved within a brittle material. The micro structures are then infiltrated with polyurethane to create the matrix or interface. More details about laser engraving technique can be found in reference [10]. The formulation is shown below

Maximize:

$$E = \frac{t}{2t + h} \frac{E_t h t}{E_t h t + L_c G_i (L_0 - h\theta)} \frac{G_i}{t h} L (L_0 - h\theta)$$

$$\sigma_s = \frac{L_0}{t + h} \tau_s$$

$$J = \frac{0.5 \tau_s u_{max} L/t}{1 - \frac{E \tau_s}{4 \sigma_s^2} \left[ \frac{u_s - L_0}{L_c} \left( \frac{L_0 \theta}{h + t} - \frac{\tau_s (u_s - L_0)}{E L_c} \right) \theta + \frac{L_0 - u_s}{t} \left( \frac{u_{max}}{L} - \frac{\tau_s (L_0 - u_s)}{t E} \right) \right]}$$

Subjected to

$$\frac{L}{t} < 0.56 \frac{K_{IC}}{\tau_s \sqrt{t}}$$

$$\frac{L_0}{t + h} > \sqrt{3}$$

$$\theta < 5^\circ$$

$$0 < \frac{L_0}{L} \leq 0.5$$

$$L \geq t$$

$$t \geq h$$

In Case IV, the optimization algorithm is allowed to find some best material properties. The notion here is to explore if there is some best blending of tablet and matrix material compositions. We do however; keep the properties within the ceramic/polymer combination. Thus, the optimal values of elastic modulus of the tablets as well as the shear modulus and the strength of the interface will be obtained from the optimization algorithm and some candidate materials can be selected accordingly. The formulation is shown below.

Maximize:

$$E = \frac{t}{2t + h} \frac{E_t h t}{E_t h t + L_c G_i (L_0 - h\theta)} \frac{G_i}{t h} L (L_0 - h\theta)$$

$$\sigma_s = \frac{L_0}{t + h} \tau_s$$

$$J = \frac{0.5 \tau_s u_{max} L / t}{1 - \frac{E \tau_s}{4 \sigma_s^2} \left[ \frac{u_s - L_0}{L_c} \left( \frac{L_0 \theta}{h + t} - \frac{\tau_s (u_s - L_0)}{E L_c} \right) \theta + \frac{L_0 - u_s}{t} \left( \frac{u_{max}}{L} - \frac{\tau_s (L_0 - u_s)}{t E} \right) \right]}$$

Subjected to

$$\frac{L}{t} < 0.56 \frac{K_{IC}}{\tau_s \sqrt{t}}$$

$$\frac{L_0}{t + h} > \sqrt{3}$$

$$\theta < 5^\circ$$

$$0 < \frac{L_0}{L} \leq 0.5$$

$$L \geq t$$

$$t \geq h$$

### 6.2.3. Implementation and General Description of NSGA II

After formulating the multi-objective optimization problem, MATLAB function ‘gamultiobj’ was used. More details can be found in Math works website. ‘Gamultiobj’ is based on NSGA II. General description of NSGA II is briefed in the following steps:

1. The population is initialized.
2. The population is sorted based on non-domination into fronts. The fist front is a non-dominated set. The second front is dominated by the first front and so on.

3. Rank, also called fitness, values are assigned to each individual. In addition, the crowding distance is calculated for each individual. The crowding distance is a measure of how close an individual to its neighbors. The higher average crowding distance, the better is the diversity.
4. Based on rank and crowding distance, parents are selected from the population. Parents with lesser rank and higher crowding distance are the ones selected.
5. The selected population generates offspring via crossover and mutation operators.
6. Based on non-dominate sorting, the current population and the offspring are sorted and the best individual for the new population is selected.

Then steps 3-6 are repeated until stopping criteria is met. The stopping criteria are maximum number of generation or maximum time limit or the average change in spread of the pareto front which is less than a specified tolerance. Finally, the results are plotted as stem 3D plot of stiffness, strength and toughness.

### **6.3. Results and Discussions**

For case I and II, the multi-objective optimization problem was solved assuming the constituent materials of natural nacre. Based on the mechanical property models develop above for strength, stiffness, and toughness, the remaining design variables are  $(L, t, L_o, h)$  for case I and  $(L, t, L_o, h, \theta)$  for case II. The resulted plot of optimal toughness, stiffness and strength are shown in Figure 20 and 21 for case I and II, respectively.

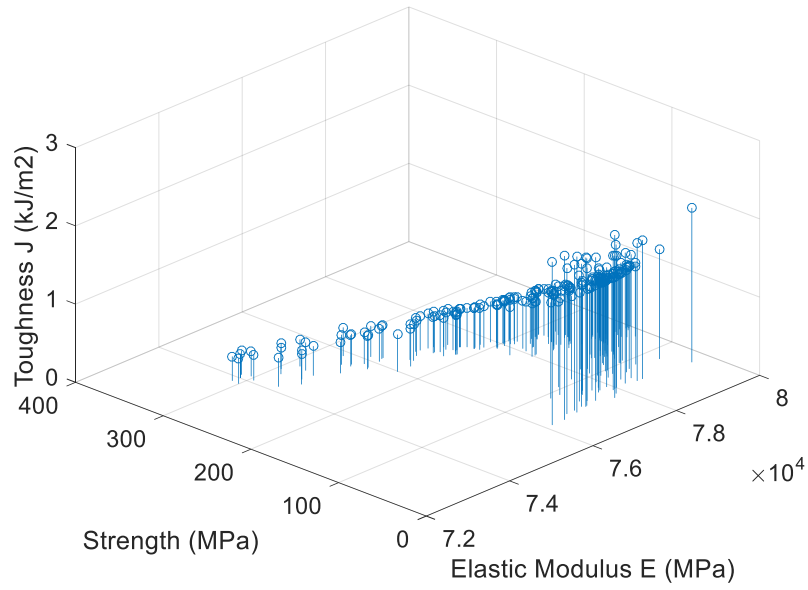


**Figure 20.** Elastic modulus (E), strength ( $\sigma$ ) and toughness (J) for case I

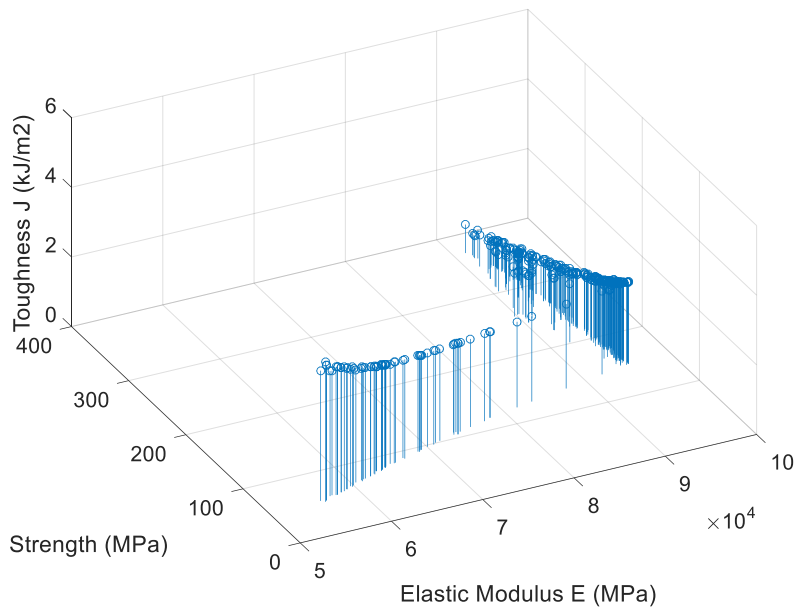


**Figure 21.** Elastic modulus (E), strength ( $\sigma$ ) and toughness (J) for case II

The range of the optimal solutions Elastic modulus ( $E$ ), strength ( $\sigma$ ) and toughness ( $J$ ) for case I and II are seen in Table 6. The design variables ( $L, t, L_o, h, \theta$ ) and their experimentally measured values are also tabulated in Table 6.

**Table 6** Comparisons of case I and II with experimental values from literature

	Case I	Case II	Experimental Values
$E(GPa)$	73.82 -80.00	55.70-95.43	40-80
$J(kJ/m^2)$	0.306-2.090	0.63-4.01	0.2-1.6
$\sigma(MPa)$	54.14-311.72	52.20-370.61	40-185
$L(\mu m)$	2.33-5.58	2.77 - 8.02	5-10
$t(\mu m)$	0.102-0.558	0.107 -0.802	0.2-0.9
$\theta (Degree)$	N/A	0-4.09°	<5°
$h(\mu m)$	10.00-14.91	10.00 -17.43	20-30
$L_o(\mu m)$	1.14-2.62	1.04 -3.84	1.6

The elastic modulus ( $E$ ) of case I is in narrower range compared to case II although both are relatively close to experimentally measured values. The toughness values ( $J$ ) for both cases are in good agreement with experimental results yet case II can achieve higher values of toughness. Strength values ( $\sigma$ ) are the same since the same equation was used for both cases and they agree with experimental values, however, high values of strength exists. Higher values of elastic modulus, strength and toughness indicate that better

properties can be obtained from nacre. Note that the optimal solution doesn't look like a surface and close to a curve this may be due to the dependence of toughness on the strength and elastic modulus of the composite.

The optimal range of tablet's length ( $L$ ), tablet's thickness ( $t$ ), and the thickness of the interface ( $h$ ) for case II is closer to experimental values than that of case I. This may be because the geometrical representation of case II is closer to actual nacre. Note that the geometrical design variables are not in the boundary as the ranges suggest. The overlap length  $L_o$  obtained was between 1.14-2.62  $\mu\text{m}$  which agrees with the optimal overlap length obtained from microscopy characterization of 1.6  $\mu\text{m}$ . Note that introducing the angle resulted in higher values of toughness. This is expected since waviness is one of the reasons for the high toughness of nacre. If not included in a design model, the toughness would be less.

For case III, the multi-objective optimization problem was solved for the borosilicate glass with polyurethane. The resulted elastic modulus, toughness and strength, shown in Figure 22, are in the ranges 724.73-764.29 MPa, 2.34-3.66  $\text{kJ/m}^2$  and 18.39-30.92 MPa, respectively. The length and thickness of tablets range from 74.39-125.22  $\mu\text{m}$ , 11.03-31.25  $\mu\text{m}$ , respectively. The thickness of the interface is around 1  $\mu\text{m}$ . The dovetail angle is between 0-2  $^\circ$ . The overlap length is 37.18-59.31  $\mu\text{m}$ . For comparison, the designed nacre-like material was with dimension of  $L = 300 \mu\text{m}$ ,  $t = 150 \mu\text{m}$ ,  $\theta = 5^\circ$ ,  $h = 2 \mu\text{m}$ ,  $L_o = L_c = L/2$  and had the stiffness, strength and toughness of 667 MPa, 10 MPa, and  $2.15 \pm 0.28 \text{ kJ/m}^2$ , respectively [10]. As noticed, the designed nacre-like material has less mechanical properties. Thus using the optimization algorithm before

designing a nacre-like material will help the designer to select the best geometry of the tablets and interface for better mechanical properties. In addition, this validates our earlier work on stiffness and toughness waviness models illustrated in section 4 and 5.

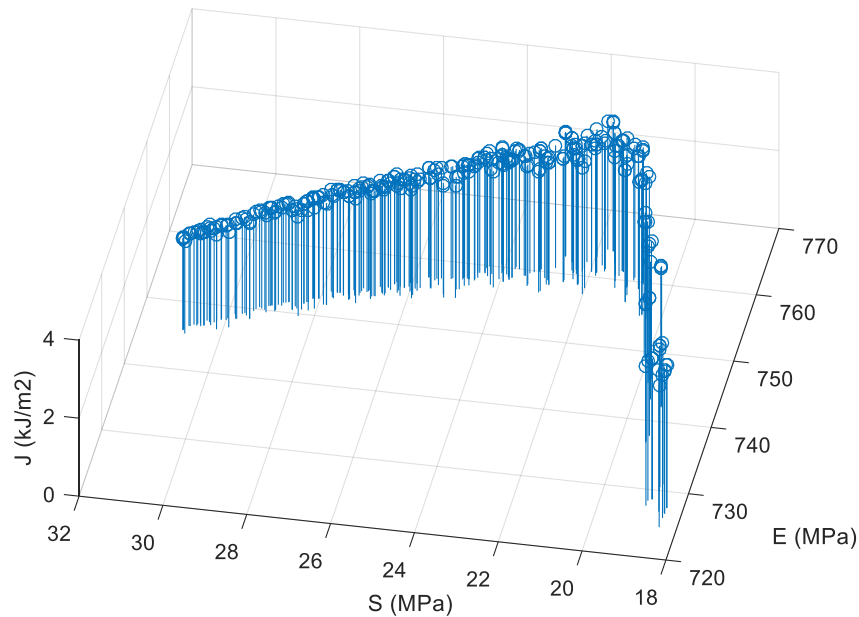


**Figure 22.** Elastic modulus (E), strength ( $\sigma$ ) and toughness (J) for case III

For case IV, the multi-objective optimization problem is solved considering a ceramic material as a tablet and a polymer material as a matrix. The design variables include geometrical and material properties. The geometrical design variables are  $(L, t, \theta, L_o, h)$  while the material design variables include  $(\tau_s, G_i \text{ \& } E_t)$ . The Pareto surface of the optimal bulk material behavior is shown in Figure 23.

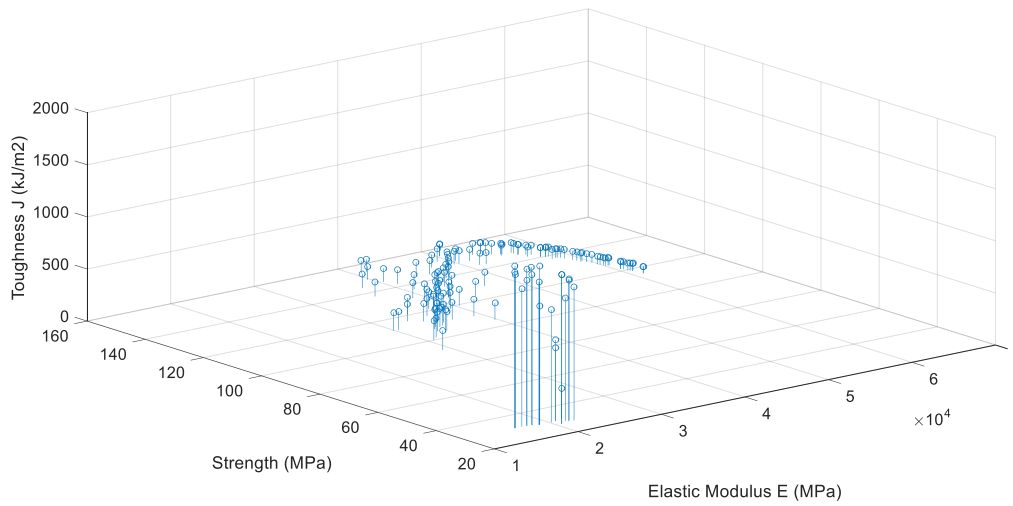


**Figure 23.** Elastic modulus (E), strength ( $\sigma$ ) and toughness (J) for case IV

The optimal elastic modulus is in the range of 16.27-61.13 GPa, the optimal toughness is 64.74-1553.9 kJ/m<sup>2</sup> and the optimal strength is 27.39-154.76 MPa. The ranges of  $L$ ,  $t$ ,  $\theta$ ,  $L_o$ ,  $h$ ,  $\tau_s$ ,  $G_i$  &  $E_t$  are shown in Table 7. The results suggest that the elastic modulus of tablet is in the range of 38.67-69.14 GPa. This implies some candidate materials for the tablets to be glass, silica, pottery, cement and concrete. From the shear modulus and shear strength, the elastic modulus and the shear strength of the interface can be calculated as shown in Table 7. Hence, the recommended polymers are polyvinyl chloride (PVC), polyethylene, and fluorocarbon polymer. Note that in order to obtain very high value of toughness, the composite sacrifices its strength and stiffness.

**Table 7** Optimal design variables data obtained from multi-objective optimization algorithm

Design Variables	Values
$L (\mu m)$	478.55-716.26
$t (\mu m)$	1.7033-6.0886
$\theta (Degree)$	7.3255-15.4634
$h (\mu m)$	1.0013 -1.4402
$L_o (\mu m)$	66.5323-243.5980
$G_i (MPa)$	59.5010-171.5705 corresponding $E_i (GPa) = 0.1547 - 0.5147$
$\tau_s (MPa)$	1.2219-3.4212 corresponding $\sigma_i (MPa) = 2.1116 - 5.925$
$E_t (GPa)$	38.6676-69.1442

In order to show the performance of the optimization algorithm, several points are selected and their corresponding objectives and design variables are shown in Table 8.

**Table 8** Optimal design variables for randomly selected five points

	Point	Point 2	Point 3	Point 4	Point 5
$E (GPa)$	20.23	20.9	30.72	47.17	60.72
$J (kJ/m^2)$	1079	696.9	184.2	121.4	67.9
$\sigma (MPa)$	29.82	30.27	100.3	148.3	119.7
$L (\mu m)$	661.1	657.8	716.3	507.4	480.2
$t (\mu m)$	2.193	2.101	1.705	1.961	5.638

**Table 8 Continued**

	<b>Point</b>	<b>Point 2</b>	<b>Point 3</b>	<b>Point 4</b>	<b>Point 5</b>
<b><math>\theta</math> (Degree)</b>	11.2	11.49	10.52	10.41	15.46
<b><math>h(\mu\text{m})</math></b>	1.17	1.151	1.01	1.033	67.9
<b><math>L_o(\mu\text{m})</math></b>	66.97	66.53	222.4	240.1	240.2
<b><math>G_i</math> (MPa)</b>	70.86	76.2	59.68	124.8	168.6
<b><math>\tau_s</math> (MPa)</b>	1.497	1.48	1.225	1.85	3.32
<b><math>E_t</math> (GPa)</b>	48.07	49.8	55.72	63.79	68.91

The points are plotted in Ashby chart of Fracture toughness vs. elastic modulus as shown in Figure 24. In this chart, the designer is interested in having a material with high modulus which means the deflections are small. In addition, high fracture toughness indicates the high load capacity of the structure can support. As can be seen, all of the five points outperform their basic constituents (ceramic and polymer) in terms of elastic modulus and fracture toughness. Points 1-4 outperform engineering composites in terms of fracture toughness while point 5 has a fracture toughness value as good as some engineering composites and alloys.



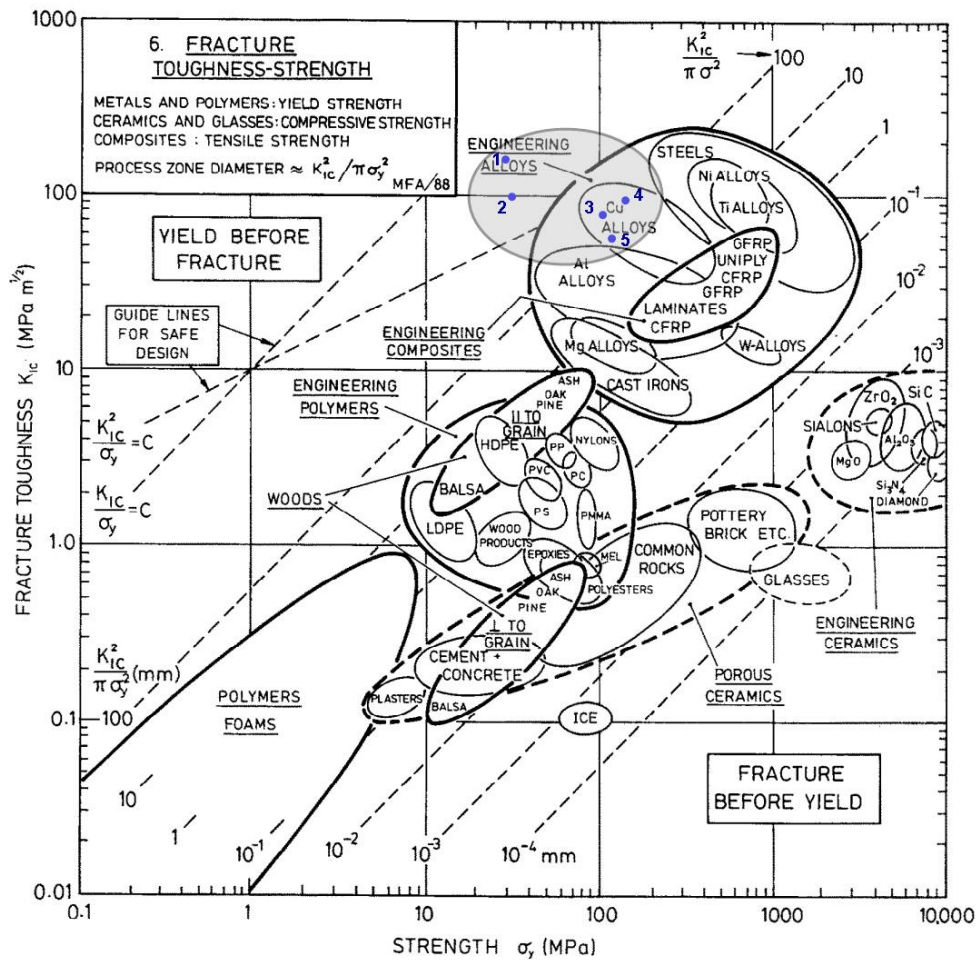


**Figure 25.** Ashby chart of fracture toughness vs. strength. Adapted with permission from [124].

Moreover, the points are plotted in Ashby chart of modulus vs. strength as shown in Figure 26. In this plot, all the points have comparable performances to engineering alloys.

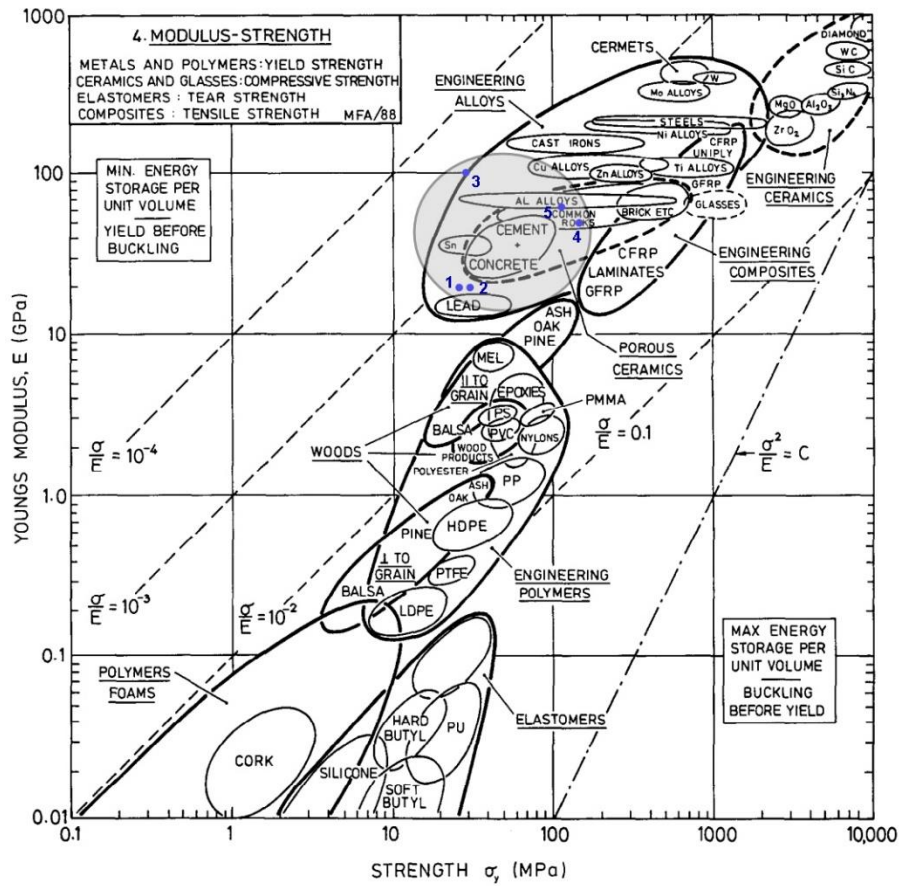


**Figure 26.** Ashby chart of elastic modulus vs. strength. Adapted with permission from [124].

The density of the nacre-like material depends on the volume fraction of the platelet and the interface. The volume fraction of the platelet is very high around 0.98. Using this value and the density of porous ceramic materials which is in the range of (2-4) Mg/m<sup>3</sup>. The density of the nacre-like material will be 1.978-3.97 (Mg/m<sup>3</sup>). Therefore, all of the five points will approximately lay in the shades squares in the Ashby plots of Elastic modulus, Strength and Fracture toughness vs. density are shown in Figures 27, 28 and 29, respectively.



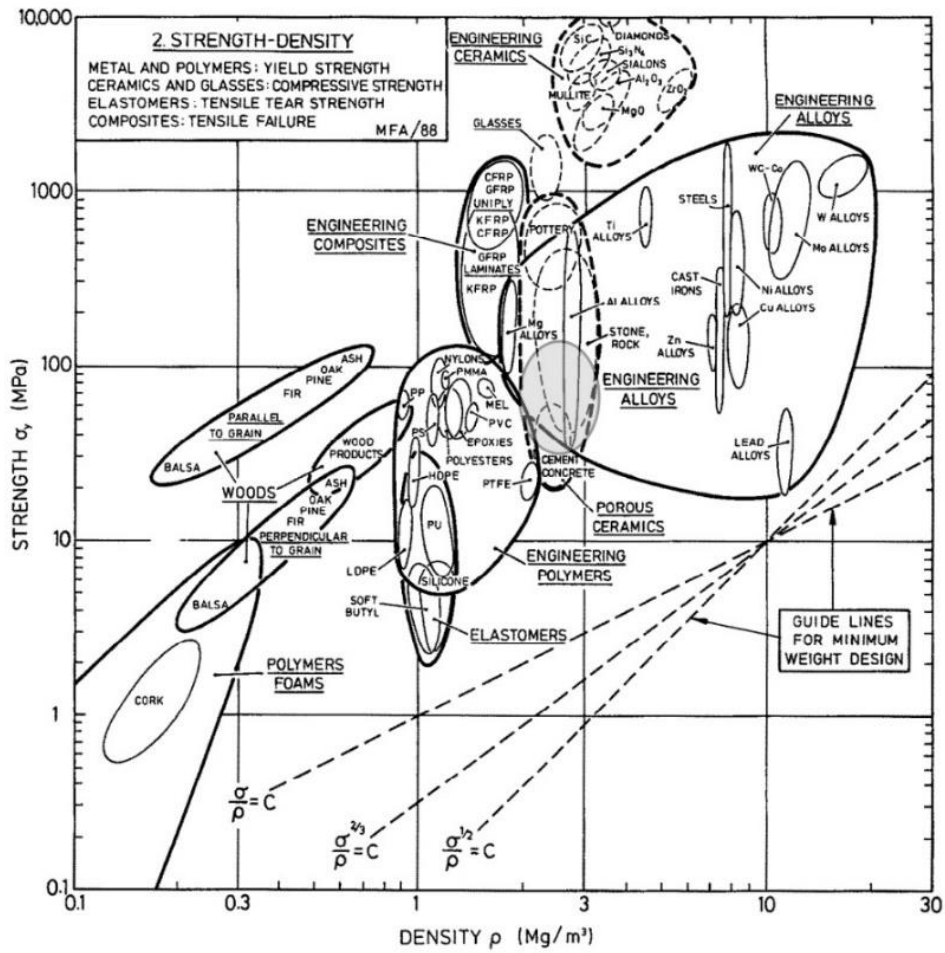
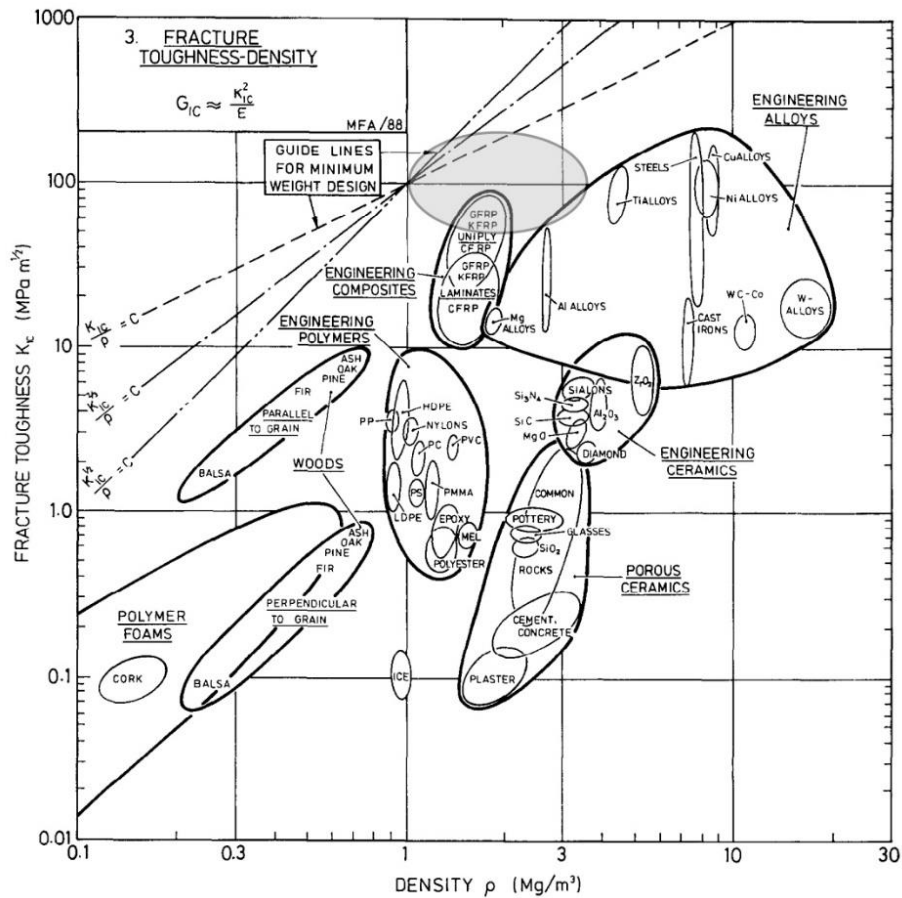


Figure 28. Ashby chart of strength vs. density. Adapted with permission from [124].



**Figure 29.** Fracture toughness vs. density. Adapted with permission from [124].

Figures 27, 28 and 29 suggest that the density of nacre-like material is as porous ceramic materials. In addition, the figures illustrate that nacre-like material is better or equivalent to some engineering alloys in terms of fracture toughness and have less density that is less weight. This indicates the potential of using nacre-like materials instead of some alloys in applications that require less weight.

## 7. CONCLUSIONS, CONTRIBUTIONS AND LIMITATIONS\*

Nacre has a desirable combination of stiffness, strength and toughness that is unachieved by any engineering materials. The main findings of this work is shown in section 7.1. Following that, the contributions and limitations can be found in section 7.2.

### 7.1. Conclusion

The main findings can be summarized in the following points.

- An improved mathematical model is presented to estimate the stiffness of nacre and nacre-like materials given properties of its main constituents including the waviness of the tablet geometry. Tablet waviness has not been addressed in many earlier models. Including the waviness shows an improved estimation of stiffness. The improved stiffness estimation is clear when comparing model results with experimental data for nacre and for a borosilicate glass with polyurethane. The model developed here also captures strain hardening that insures high spreading of nonlinear deformations. High spreading of nonlinear deformations result in high values of toughness.
- A waviness toughness model for nacre and nacre-like materials was developed in which toughness is quantified and the R-curve is obtained. The model captures the toughness due to bridging and process zone toughening mechanisms. Applying the

---

\*Part of this section is reprinted with permission from, "Modeling of a biological material nacre: Waviness stiffness model," by Authors' N. S. Al-Maskari, D. A. McAdams, and J. N. Reddy, 2017. *Materials Science and Engineering: C*, vol. 70, Part 1, pp. 772-776, Copyright 2016 by Elsevier B.V.

model to nacre and a nacre-like material of Alumina/PMMA results in R-curve close to the one obtained experimentally and toughness values is lower than experimental due to the other toughening mechanisms that are not considered.

- A multi-objective optimization problem is formulated and solved using the well-known genetic algorithm NSGA II. Four cases were considered in which three of them are considered to be geometrical optimization. In the three cases the materials are known and only geometrical design variables are optimized for maximum stiffness, toughness and strength. For case I and II, the material considered is the actual constituents of nacre where case I is for flat tablets and case II is for wavy tablets. The optimal elastic modulus, strength and toughness are in good agreement with data found in literature for nacre with wider range for case II. Case II toughness values are higher than case I and closer to experimental results. This is expected since case II includes the waviness that is one of the reasons of high toughness values found for nacre. For both cases the geometrical design variables obtained for case II is closer than case I to experimental values found for nacre. Indicating that including the waviness better resembles actual nacre. In addition, the two cases validates the waviness stiffness and toughness models developed here. For case III, the optimization algorithm was implemented using the data of a nacre-like material of borosilicate-glass with polyurethane. The resulted optimal stiffness, strength and toughness exceeds the designed once. This indicates that running the optimization algorithm prior to the design stage is crucial. For case IV,

the mechanical properties of optimized nacre-like material are remarkable and some of them are close to engineering alloys although the constituents are made of ceramic and polymer. In addition, it has low density similar to porous ceramics making them suitable for lightweight designs and applications. This demonstrates the potential of nacre-like materials and reveals the reasons behind studying and trying to mimic nacre.

## **7.2. Contributions and Limitations**

The designer will be able to input the material properties and geometries of the tablet and interface and predict via the models the material's stiffness as well as its toughness as crack grows. These models differ from earlier models since the waviness of the tablets have been included that have been shown to increase the toughness of nacre and nacre-like materials. Having parametric models allow a material designer to easily explore a trade space of different material compositions and geometries to find suitable, or perhaps optimal materials for specific applications.

After understanding the main principles that lead to nacre's remarkable properties and being able to model those and combine them with a large number of existing materials to produce new nacre-like materials as well as expand the application of the current ones, it is desirable to have an algorithm that suggests some candidate materials and geometry of the staggered structure. Hence there is a need for a multi-objective optimization algorithm in which the algorithm can suggest the candidate material with the optimal geometrical dimensions of the structure that lead to optimal stiffness, strength and toughness. However, the material is limited to ceramic/polymer material at this stage and

can be developed to include different materials, e.g. alloys, metals and polymers, provided that toughness predication is developed for different types of materials.

Nacre like-materials are useful in areas such as material science, biomaterials development, civil, petroleum and nanotechnology [18] in which ceramic materials and composites can be replaced with nacre-like materials in applications that require high stiffness and toughness with less weight. Nacre-like materials and coatings have been developed for biomedical applications such as development of better performance implant materials [19]. In addition, researchers are looking into using cement paste, which is concrete's binding ingredient, with the structure and properties of natural materials such as nacre, bone and deep-sea sponge [20].

## 8. SUGGESTED FUTURE WORK

For future work, the followings are suggested:

- The model can be generalized to include tablets made from different materials. For example the overlapping tablets can be from different materials. This may results in new materials with more desired properties that can be used in different applications.
- Additional toughening mechanisms can be included for improved toughness prediction. For the case of ceramic tablets, these toughening mechanisms includes; crack deflection and intrinsic toughening mechanism.
- Toughening mechanisms for non-ceramic tablets may be included as well.
- Toughening mechanisms can occur at different length scales other than micro due to the hierarchical structure of nacre. These can be included in the toughness model as well as optimization algorithm.
- Synthesize nacre-like materials as suggested from multi-objective optimization algorithm in order to assess the performance of the algorithm.

## REFERENCES

- [1] M. A. Meyers, P.-Y. Chen, A. Y.-M. Lin, and Y. Seki, "Biological materials: structure and mechanical properties," *Progress in Materials Science*, vol. 53, pp. 1-206, 2008.
- [2] M. A. Meyers, A. Y. M. Lin, Y. Seki, P.-Y. Chen, B. K. Kad, and S. Bodde, "Structural biological composites: an overview," *The Journal of The Minerals, Metals & Materials Society*, vol. 58, pp. 35-41, 2006.
- [3] X. Wei, M. Naraghi, and H. D. Espinosa, "Optimal length scales emerging from shear load transfer in natural materials: application to carbon-based nanocomposite design," *ACS Nano*, vol. 6, pp. 2333-2344, 2012.
- [4] F. Barthelat, H. Tang, P. D. Zavattieri, C. M. Li, and H. D. Espinosa, "On the mechanics of mother-of-pearl: a key feature in the material hierarchical structure," *Journal of the Mechanics and Physics of Solids*, vol. 55, pp. 306-337, 2007.
- [5] D. Zhu and F. Barthelat, "A Novel biomimetic material duplicating the structure and mechanics of natural nacre," in *Mechanics of Biological Systems and Materials, Volume 2*, T. Proulx, Ed., ed: Springer New York, 2011, pp. 181-187.
- [6] M. Sarikaya, "An introduction to biomimetics: a structural viewpoint," *Microscopy Research and Technique*, vol. 27, pp. 360-375, 1994.
- [7] H. D. Espinosa, A. L. Juster, F. J. Latourte, O. Y. Loh, D. Gregoire, and P. D. Zavattieri, "Tablet-level origin of toughening in abalone shells and translation to synthetic composite materials," *Nature Communications*, vol. 2, pp. 173, 2011.
- [8] P.-Y. Chen, J. McKittrick, and M. A. Meyers, "Biological materials: functional adaptations and bioinspired designs," *Progress in Materials Science*, vol. 57, pp. 1492-1704, 2012.
- [9] C. Zhang, D. A. Mcadams and a. G. J. Grunlan, "Nano/micro-manufacturing of bioinspired materials: a review of methods to mimic natural structures," *Advanced Materials*, vol. 28, pp. 6292-6321, 2016.
- [10] M. Mirkhalaf and F. Barthelat, "A laser-engraved glass duplicating the structure, mechanics and performance of natural nacre," *Bioinspiration & Biomimetics*, vol. 10, pp. 026005, 2015.

- [11] E. Munch, M. E. Launey, D. H. Alsem, E. Saiz, A. P. Tomsia, and R. O. Ritchie, "Tough, bio-inspired hybrid materials," *Science*, vol. 322, pp. 1516-1520, 2008.
- [12] H. Bai, F. Walsh, B. Gludovatz, B. Delattre, C. Huang, Y. Chen, A. P. Tomsia and R. O. Ritchie, "Bioinspired hydroxyapatite/poly(methyl methacrylate) composite with a nacre-mimetic architecture by a bidirectional freezing method," *Advanced Materials*, vol. 28, pp. 50-56, 2016.
- [13] P. Podsiadlo, A. K. Kaushik, E. M. Arruda, A. M. Waas, B. S. Shim, J. Xu, *et al.*, "Ultrastrong and stiff layered polymer nanocomposites," *Science*, vol. 318, p. 80, 2007.
- [14] M. Mirkhalaf and F. Barthelat, "Nacre-like materials using a simple doctor blading technique: fabrication, testing and modeling," *Journal of the Mechanical Behavior of Biomedical Materials*, vol. 56, pp. 23-33, 2016.
- [15] K. Brandt, M. F. H. Wolff, V. Salikov, S. Heinrich, and G. A. Schneider, "A novel method for a multi-level hierarchical composite with brick-and-mortar structure," *Scientific Reports*, vol. 3, pp. 2322, 2013.
- [16] G. Mayer, "Rigid biological systems as models for synthetic composites," *Science*, vol. 310, pp. 1144-1147, 2005.
- [17] A. Walther, I. Bjurhager, J.-M. Malho, J. Pere, J. Ruokolainen, L. A. Berglund, *et al.*, "Large-area, lightweight and thick biomimetic composites with superior material properties via fast, economic, and green pathways," *Nano Letters*, vol. 10, pp. 2742-2748, 2010.
- [18] U. G. K. Wegst, H. Bai, E. Saiz, A. P. Tomsia, and R. O. Ritchie, "Bioinspired structural materials," *Nature Materials*, vol. 14, pp. 23-36, 2015.
- [19] G. M. Luz and J. F. Mano, "Biomimetic design of materials and biomaterials inspired by the structure of nacre," *Philosophical Transactions of the Royal Society of London A: Mathematical, Physical and Engineering Sciences*, vol. 367, pp. 1587-1605, 2009.
- [20] S. D. Palkovic, D. B. Brommer, K. Kupwade-Patil, A. Masic, M. J. Buehler, and O. Büyüköztürk, "Roadmap across the mesoscale for durable and sustainable cement paste: a bioinspired approach," *Construction and Building Materials*, vol. 115, pp. 13-31, 2016.
- [21] U. G. K. Wegst and M. F. Ashby, "The mechanical efficiency of natural materials," *Philosophical Magazine*, vol. 84, pp. 2167-2186, 2004.

- [22] M. F. Ashby, L. J. Gibson, U. Wegst, and R. Olive, "The mechanical properties of natural materials. I. material property charts," *Proceedings of the Royal Society of London A: Mathematical, Physical and Engineering Sciences*, vol. 450, pp. 123-140, 1995.
- [23] F. Barthelat and R. Rabiei, "Toughness amplification in natural composites," *Journal of the Mechanics and Physics of Solids*, vol. 59, pp. 829-840, 2011.
- [24] M. A. Meyers, P.-Y. Chen, M. I. Lopez, Y. Seki and A. Y.-M. Lin, "Biological materials: a materials science approach," *Journal of the Mechanical Behavior of Biomedical Materials*, vol. 4, pp. 626 - 657, 2011.
- [25] F. Barthelat, J. E. Rim, and H. D. Espinosa, "A review on the structure and mechanical properties of mollusk shells – perspectives on synthetic biomimetic materials," in *Applied Scanning Probe Methods XIII*, B. Bhushan and H. Fuchs, Eds., ed: Springer Berlin Heidelberg, pp. 17-44, 2009.
- [26] H. D. Espinosa, J. E. Rim, F. Barthelat, and M. J. Buehler, "Merger of structure and material in nacre and bone – perspectives on de novo biomimetic materials," *Progress in Materials Science*, vol. 54, pp. 1059-1100, 2009.
- [27] J. Sun and B. Bhushan, "Hierarchical structure and mechanical properties of nacre: a review," *Royal Society of Chemistry Advances*, vol. 2, pp. 7617-7632, 2012.
- [28] F. D. Fleischli, M. Dietiker, C. Borgia, and R. Spolenak, "The influence of internal length scales on mechanical properties in natural nanocomposites: a comparative study on inner layers of seashells," *Acta Biomaterialia*, vol. 4, pp. 1694-1706, 2008.
- [29] J. Machado, M. Lopes-Lima, A. Damasceno-Oliveira, A. Colaço, J. Andrade, D. Silva, C. Jiménez-López, A. Rodríguez-Navarro and A. Checa "The influence of hydrostatic pressure on shell mineralization of anodonta cygnea: a comparative study with a hydrothermal vent bivalve bathymodiolus azoricus," *Journal of Shellfish Research*, vol. 28, pp. 899-904, 2009.
- [30] H. M. Leung and S. K. Sinha, "Scratch and indentation tests on seashells," *Tribology International*, vol. 42, pp. 40-49, 2009.
- [31] B. Pokroy, V. Demensky, and E. Zolotoyabko, "Nacre in mollusk shells as a multilayered structure with strain gradient," *Advanced Functional Materials*, vol. 19, pp. 1054-1059, 2009.

- [32] H. Moshe-Drezner, D. Shilo, A. Dorogoy, and E. Zolotoyabko, "Nanometer-scale mapping of elastic modules in biogenic composites: the nacre of mollusk shells," *Advanced Functional Materials*, vol. 20, pp. 2723-2728, 2010.
- [33] J. D. Currey, "Mechanical properties of mother of pearl in tension," *Proceedings of the Royal Society of London. Series B, Biological Sciences*, vol. 196, pp. 443-463, 1977.
- [34] J. H. E. Cartwright and A. G. Checa, "The dynamics of nacre self-assembly," *Journal of The Royal Society Interface*, vol. 4, p. 491, 2007.
- [35] A. G. Checa, J. H. E. Cartwright, and M.-G. Willinger, "Mineral bridges in nacre," *Journal of Structural Biology*, vol. 176, pp. 330-339, 2011.
- [36] A. G. Checa, J. H. E. Cartwright, and M.-G. Willinger, "The key role of the surface membrane in why gastropod nacre grows in towers," *Proceedings of the National Academy of Sciences*, vol. 106, pp. 38-43, 2009.
- [37] F. Nudelman, B. A. Gotliv, L. Addadi, and S. Weiner, "Mollusk shell formation: Mapping the distribution of organic matrix components underlying a single aragonitic tablet in nacre," *Journal of Structural Biology*, vol. 153, pp. 176-187, 2006.
- [38] J. H. E. Cartwright, A. G. Checa, B. Escibano, and C. I. Sainz-Díaz, "Spiral and target patterns in bivalve nacre manifest a natural excitable medium from layer growth of a biological liquid crystal," *Proceedings of the National Academy of Sciences*, vol. 106, pp. 10499-10504, 2009.
- [39] P. Stempflé and M. Brendlé, "Tribological behaviour of nacre: influence of the environment on the elementary wear processes," *Tribology International*, vol. 39, pp. 1485-1496, 2006.
- [40] P. Stempflé, O. Pantalé, M. Rousseau, E. Lopez, and X. Bourrat, "Mechanical properties of the elemental nanocomponents of nacre structure," *Materials Science and Engineering: C*, vol. 30, pp. 715-721, 2010.
- [41] R. Z. Wang, Z. Suo, A. G. Evans, N. Yao, and I. A. Aksay, "Deformation mechanisms in nacre," *Journal of Materials Research*, vol. 16, pp. 2485-2493, 2001.
- [42] D. Chateigner, C. Hedegaard, and H. R. Wenk, "Mollusc shell microstructures and crystallographic textures," *Journal of Structural Geology*, vol. 22, pp. 1723-1735, 2000.

- [43] J. D. Currey, P. Zioupos, P. Davies, and A. Casino, "Mechanical properties of nacre and highly mineralized bone," *Proceedings. Biological sciences: The Royal Society*, vol. 268, pp. 107-111, 2001.
- [44] A. P. Jackson, J. F. V. Vincent, and R. M. Turner, *The mechanical design of nacre*, vol. 234, 1988.
- [45] M. Rousseau, E. Lopez, A. Couté, G. Mascarel, D. C. Smith, R. Naslain, *et al.*, "Sheet nacre growth mechanism: a voronoi model," *Journal of Structural Biology*, vol. 149, pp. 149-157, 2005.
- [46] F. Ren, X. Wan, Z. Ma, and J. Su, "Study on microstructure and thermodynamics of nacre in mussel shell," *Materials Chemistry and Physics*, vol. 114, pp. 367-370, 2009.
- [47] F. Song, J. Zhou, X. Xu, Y. Xu, and Y. Bai, "Effect of a negative poisson ratio in the tension of ceramics," *Physical Review Letters*, vol. 100, pp. 245502, 2008.
- [48] J.-y. Sun and J. Tong, "Fracture toughness properties of three different biomaterials measured by nanoindentation," *Journal of Bionic Engineering*, vol. 4, pp. 11-17, 2007.
- [49] A. Lin and M. A. Meyers, "Growth and structure in abalone shell," *Materials Science and Engineering: A*, vol. 390, pp. 27-41, 2005.
- [50] M. A. Meyers, A. Y.-M. Lin, P.-Y. Chen, and J. Muyor, "Mechanical strength of abalone nacre: role of the soft organic layer," *Journal of the Mechanical Behavior of Biomedical Materials*, vol. 1, pp. 76-85, 2008.
- [51] M. A. Meyers, C. T. Lim, A. Li, B. R. Hairul Nizam, E. P. S. Tan, Y. Seki, and J. McKittrick, "The role of organic intertile layer in abalone nacre," *Materials Science and Engineering: C*, vol. 29, pp. 2398-2410, 2009.
- [52] F. Heinemann, M. Launspach, K. Gries, and M. Fritz, "Gastropod nacre: structure, properties and growth — biological, chemical and physical basics," *Biophysical Chemistry*, vol. 153, pp. 126-153, 2011.
- [53] F. Song, A. K. Soh, and Y. L. Bai, "Structural and mechanical properties of the organic matrix layers of nacre," *Biomaterials*, vol. 24, pp. 3623-3631, 2003.
- [54] F. Song, X. H. Zhang, and Y. L. Bai, "Microstructure and characteristics in the organic matrix layers of nacre," *Journal of Materials Research*, vol. 17, pp. 1567-1570, 2002.

- [55] S. Blank, M. Arnoldi, S. Khoshnavaz, L. Treccani, M. Kuntz, K. Mann, G. Grathwohl and M. Fritz, "The nacre protein perlucin nucleates growth of calcium carbonate crystals," *Journal of Microscopy*, vol. 212, pp. 280-291, 2003.
- [56] F. Barthelat, C.-M. Li, C. Comi, and H. D. Espinosa, "Mechanical properties of nacre constituents and their impact on mechanical performance," *Journal of Materials Research*, vol. 21, pp. 1977-1986, 2006.
- [57] J. Bezares, R. J. Asaro, and M. Hawley, "Macromolecular structure of the organic framework of nacre in *Haliotis rufescens*: implications for growth and mechanical behavior," *Journal of Structural Biology*, vol. 163, pp. 61-75, 2008.
- [58] B. Jiddu, P. Zhangli, A. Robert , and Z. Qiang, "Macromolecular structure and viscoelastic response of the organic framework of nacre in *Haliotis rufescens*: a perspective and overview," *Theoretical and Applied Mechanics*, 2011.
- [59] M. Fritz, A. M. Belcher, M. Radmacher, D. A. Walters, P. K. Hansma, G. D. Stucky, D.E. Morse and S. Mann, "Flat pearls from biofabrication of organized composites on inorganic substrates," *Nature*, vol. 371, pp. 49-51, 1994.
- [60] X. Li, Z.-H. Xu, and R. Wang, "In situ observation of nanograin rotation and deformation in nacre," *Nano Letters*, vol. 6, pp. 2301-2304, 2006.
- [61] X. Li, W.-C. Chang, Y. J. Chao, R. Wang, and M. Chang, "Nanoscale structural and mechanical characterization of a natural nanocomposite material: the shell of red abalone," *Nano Letters*, vol. 4, pp. 613-617, 2004.
- [62] A. Y.-M. Lin, P.-Y. Chen, and M. A. Meyers, "The growth of nacre in the abalone shell," *Acta Biomaterialia*, vol. 4, pp. 131-138, 2008.
- [63] A. Y.-M. Lin and M. A. Meyers, "Interfacial shear strength in abalone nacre," *Journal of the Mechanical Behavior of Biomedical Materials*, vol. 2, pp. 607-612, 2009.
- [64] K. S. Katti, D. R. Katti, S. M. Pradhan, and A. Bhosle, "Platelet interlocks are the key to toughness and strength in nacre," *Journal of Materials Research*, vol. 20, pp. 1097-1100, 2005.
- [65] K. S. Katti, B. Mohanty, and D. R. Katti, "Nanomechanical properties of nacre," *Journal of Materials Research*, vol. 21, pp. 1237-1242, 2006.
- [66] R. Menig, M. H. Meyers, M. A. Meyers, and K. S. Vecchio, "Quasi-static and dynamic mechanical response of *Haliotis rufescens* (abalone) shells," *Acta Materialia*, vol. 48, pp. 2383-2398, 2000.

- [67] M. A. Meyers and K. K. Chawla, *Mechanical Behavior of Materials*: Cambridge University Press, 2008.
- [68] B. Mohanty, K. S. Katti, D. R. Katti, and D. Verma, "Dynamic nanomechanical response of nacre," *Journal of Materials Research*, vol. 21, pp. 2045-2051, 2006.
- [69] T. E. Schäffer, C. Ionescu-Zanetti, R. Proksch, M. Fritz, D. A. Walters, N. Almqvist, C. M. Zaremba, A. M. Belcher, B. L. Smith, G. D. Stucky, D. E. Morse and P. K. Hansma, "Does abalone nacre form by heteroepitaxial nucleation or by growth through mineral bridges?," *Chemistry of Materials*, vol. 9, pp. 1731-1740, 1997.
- [70] D. Verma, K. Katti, and D. Katti, "Nature of water in nacre: A 2D fourier transform infrared spectroscopic study," *Spectrochimica Acta Part A: Molecular and Biomolecular Spectroscopy*, vol. 67, pp. 784-788, 2007.
- [71] N. Yao, A. Epstein, and A. Akey, "Crystal growth via spiral motion in abalone shell nacre," *Journal of Materials Research*, vol. 21, pp. 1939-1946, 2006.
- [72] M. Yourdkhani, D. Pasini, and F. Barthelat, "Multiscale mechanics and optimization of gastropod shells," *Journal of Bionic Engineering*, vol. 8, pp. 357-368, 2011.
- [73] C. M. Zaremba, A. M. Belcher, M. Fritz, Y. Li, S. Mann, P. K. Hansma, D. E. Morse, J. S. Speck and G. D. Stuck, "Critical transitions in the biofabrication of abalone shells and flat pearls," *Chemistry of Materials*, vol. 8, pp. 679-690, 1996.
- [74] R. Menig, M. H. Meyers, M. A. Meyers, and K. S. Vecchio, "Quasi-static and dynamic mechanical response of *Strombus gigas* (conch) shells," *Materials Science and Engineering: A*, vol. 297, pp. 203-211, 2001.
- [75] B. J. F. Bruet, H. J. Qi, M. C. Boyce, R. Panas, K. Tai, L. Frick and C. Ortiz, "Nanoscale morphology and indentation of individual nacre tablets from the gastropod mollusc *trochus niloticus*," *Journal of Materials Research*, vol. 20, pp. 2400-2419, 2005.
- [76] J. D. Currey and J. D. Taylor, "The mechanical behaviour of some molluscan hard tissues," *Journal of Zoology*, vol. 173, pp. 395-406, 1974.
- [77] M. A. Meyers, P.-Y. Chen, M. I. Lopez, Y. Seki, and A. Y. M. Lin, "Biological materials: a materials science approach," *Journal of the Mechanical Behavior of Biomedical Materials*, vol. 4, pp. 626-657, 2011.
- [78] B. Francois, "Nacre from mollusk shells: a model for high-performance structural materials," *Bioinspiration & Biomimetics*, vol. 5, pp. 035001, 2010.

- [79] F. Barthelat and H. D. Espinosa, "An experimental investigation of deformation and fracture of nacre–mother of pearl," *Experimental Mechanics*, vol. 47, pp. 311-324, 2007.
- [80] M. Grujicic, S. Ramaswami, and J. Snipes, "Nacre-like ceramic/polymer laminated composite for use in body-armor applications," *AIMS Materials Science*, vol. 3, pp. 83-113, 2016.
- [81] H. Kakisawa and T. Sumitomo, "The toughening mechanism of nacre and structural materials inspired by nacre," *Science and Technology of Advanced Materials*, vol. 12, pp. 064710, 2011.
- [82] S. P. Kotha, Y. Li, and N. Guzelsu, "Micromechanical model of nacre tested in tension," *Journal of Materials Science*, vol. 36, pp. 2001-2007, 2001.
- [83] M. E. Launey, "On the fracture toughness of advanced materials," *advanced materials*, vol. 21, pp. 2103–2110, 2009.
- [84] R. Wang and H. S. Gupta, "Deformation and fracture mechanisms of bone and nacre," *Annual Review of Materials Research*, vol. 41, pp. 41-73, 2011.
- [85] R. Z. Wang, H. B. Wen, F. Z. Cui, H. B. Zhang, and H. D. Li, "Observations of damage morphologies in nacre during deformation and fracture," *Journal of Materials Science*, vol. 30, pp. 2299-2304, 1995.
- [86] R. Rabiei, S. Bekah, and F. Barthelat, "Failure mode transition in nacre and bone-like materials," *Acta Biomaterialia*, vol. 6, pp. 4081-4089, 2010.
- [87] M. Mirkhalaf, A. K. Dastjerdi, and F. Barthelat, "Overcoming the brittleness of glass through bio-inspiration and micro-architecture," *Nature Communications*, vol. 5, 2014.
- [88] R. T. Marler and J. S. Arora, "Survey of multi-objective optimization methods for engineering," *Structural and Multidisciplinary Optimization*, vol. 26, pp. 369-395, 2004.
- [89] C. C. Coello, G. B. Lamont, and D. A. van Veldhuizen, *Evolutionary algorithms for solving multi-objective problems*: Springer US, 2007.
- [90] K. Miettinen, *Nonlinear multiobjective optimization*: Springer US, 1999.
- [91] I. Das and J. Dennis, "Normal-boundary intersection: a new method for generating the pareto surface in nonlinear multicriteria optimization problems," *SIAM Journal on Optimization*, vol. 8, pp. 631-657, 1998.

- [92] R. de S. Motta, S. M. B. Afonso, and P. R. M. Lyra, "A modified NBI and NC method for the solution of N-multiobjective optimization problems," *Structural and Multidisciplinary Optimization*, vol. 46, pp. 239-259, 2012.
- [93] A. Messac and C. A. Mattson, "Normal constraint method with guarantee of even representation of complete pareto frontier," *The American Institute of Aeronautics and Astronautics Journal*, vol. 42, pp. 2101-2111, 2004.
- [94] A. Messac, A. Ismail-Yahaya, and C. A. Mattson, "The normalized normal constraint method for generating the Pareto frontier," *Structural and Multidisciplinary Optimization*, vol. 25, pp. 86-98, 2003.
- [95] D. Mueller-Gritschneider, H. Graeb, and U. Schlichtmann, "A successive approach to compute the bounded pareto front of practical multiobjective optimization problems," *SIAM Journal on Optimization*, vol. 20, pp. 915-934, 2009.
- [96] T. Erfani and S. V. Utyuzhnikov, "Directed search domain: a method for even generation of the Pareto frontier in multiobjective optimization," *Engineering Optimization*, vol. 43, pp. 467-484, 2011.
- [97] J. Horn, N. Nafpliotis, and D. E. Goldberg, "A niched Pareto genetic algorithm for multiobjective optimization," in *Evolutionary Computation, 1994. IEEE World Congress on Computational Intelligence., Proceedings of the First IEEE Conference*, vol.1, pp. 82-87, 1994.
- [98] M. Erickson, A. Mayer, and J. Horn, "The niched Pareto genetic algorithm 2 applied to the design of groundwater remediation systems," in *Evolutionary Multi-Criterion Optimization: First International Conference, EMO 2001 Zurich, Switzerland, March 7-9, 2001 Proceedings*, E. Zitzler, L. Thiele, K. Deb, C. A. Coello Coello, and D. Corne, Eds., ed Berlin, Heidelberg: Springer Berlin Heidelberg, pp. 681-695, 2001.
- [99] N. Srinivas and K. Deb, "Multiobjective optimization using nondominated sorting in genetic algorithms," *Evolutionary Computation*, vol. 2, pp. 221-248, 1994.
- [100] K. Deb, S. Agrawal, A. Pratap, and T. Meyarivan, "A fast elitist non-dominated sorting genetic algorithm for multi-objective optimization: NSGA-II," in *Parallel Problem Solving from Nature PPSN VI: 6th International Conference Paris, France, September 18-20, 2000 Proceedings*, M. Schoenauer, K. Deb, G. Rudolph, X. Yao, E. Lutten, J. J. Merelo, *et al.*, Eds., ed Berlin, Heidelberg: Springer Berlin Heidelberg, pp. 849-858, 2000.

- [101] C. A. C. Coello and G. T. Pulido, "A micro-genetic algorithm for multiobjective optimization," in *Evolutionary Multi-Criterion Optimization: First International Conference, EMO 2001 Zurich, Switzerland, March 7–9, 2001 Proceedings*, E. Zitzler, L. Thiele, K. Deb, C. A. C. Coello, and D. Corne, Eds., ed Berlin, Heidelberg: Springer Berlin Heidelberg, pp. 126-140, 2001.
- [102] G. T. Pulido and C. A. C. Coello, "The micro genetic algorithm 2: towards online adaptation in evolutionary multiobjective optimization," in *Evolutionary Multi-Criterion Optimization: Second International Conference, EMO 2003, Faro, Portugal, April 8–11, 2003. Proceedings*, C. M. Fonseca, P. J. Fleming, E. Zitzler, L. Thiele, and K. Deb, Eds., ed Berlin, Heidelberg: Springer Berlin Heidelberg, pp. 252-266, 2003.
- [103] J. K. Cochran, S.-M. Horng, and J. W. Fowler, "A multi-population genetic algorithm to solve multi-objective scheduling problems for parallel machines," *Computers & Operations Research*, vol. 30, pp. 1087-1102, 2003.
- [104] J. Knowles, "ParEGO: a hybrid algorithm with on-line landscape approximation for expensive multiobjective optimization problems," *IEEE Transactions on Evolutionary Computation*, vol. 10, pp. 50-66, 2006.
- [105] K. Deb, A. Pratap, S. Agarwal, and T. Meyarivan, "A fast and elitist multiobjective genetic algorithm: NSGA-II," *IEEE Transactions on Evolutionary Computation*, vol. 6, pp. 182-197, 2002.
- [106] G. E. Padawer and N. Beecher, "On the strength and stiffness of planar reinforced plastic resins," *Polymer Engineering & Science*, vol. 10, pp. 185--192, 1970.
- [107] Z. Q. Zhang, B. Liu, Y. Huang, K. C. Hwang, and H. Gao, "Mechanical properties of unidirectional nanocomposites with non-uniformly or randomly staggered platelet distribution," *Journal of the Mechanics and Physics of Solids*, vol. 58, pp. 1646-1660, 2010.
- [108] B. Bar-On and H. D. Wagner, "New insights into the Young's modulus of staggered biological composites," *Materials Science and Engineering: C*, vol. 33, pp. 603-607, 2013.
- [109] B. Bar-On and H. D. Wagner, "Mechanical model for staggered bio-structure," *Journal of the Mechanics and Physics of Solids*, vol. 59, pp. 1685-1701, 2011.
- [110] M. R. Begley, N. R. Philips, B. G. Compton, D. V. Wilbrink, R. O. Ritchie, and M. Utz, "Micromechanical models to guide the development of synthetic 'brick and mortar' composites," *Journal of the Mechanics and Physics of Solids*, vol. 60, pp. 1545-1560, 2012.

- [111] A. Dutta, S. A. Tekalur, and M. Miklavcic, "Optimal overlap length in staggered architecture composites under dynamic loading conditions," *Journal of the Mechanics and Physics of Solids*, vol. 61, pp. 145-160, 2013.
- [112] N. Sakhavand and R. Shahsavari, "Universal composition–structure–property maps for natural and biomimetic platelet–matrix composites and stacked heterostructures," *Nature Communications*, vol. 6, 2015.
- [113] N. S. Al-Maskari, D. A. McAdams, and J. N. Reddy, "Modeling of a biological material nacre: waviness stiffness model," *Materials Science and Engineering: C*, vol. 70, Part 1, pp. 772-776, 2017.
- [114] K. Okumura and P. G. deGennes, "Why is nacre strong? Elastic theory and fracture mechanics for biocomposites with stratified structures," *The European Physical Journal E*, vol. 4, pp. 121-127, 2001.
- [115] H. Gao, B. Ji, M. J. Buehler, and H. Yao, "Flaw tolerant bulk and surface nanostructures of biological systems," *Mechanics & chemistry of biosystems : MCB*, vol. 1, pp. 37-52, 2004.
- [116] B. Ji and H. Gao, "Mechanical properties of nanostructure of biological materials," *Journal of the Mechanics and Physics of Solids*, vol. 52, pp. 1963-1990, 2004.
- [117] Y. Shao, H.-P. Zhao, X.-Q. Feng, and H. Gao, "Discontinuous crack-bridging model for fracture toughness analysis of nacre," *Journal of the Mechanics and Physics of Solids*, vol. 60, pp. 1400-1419, 2012.
- [118] F. Barthelat, "Designing nacre-like materials for simultaneous stiffness, strength and toughness: optimum materials, composition, microstructure and size," *Journal of the Mechanics and Physics of Solids*, vol. 73, pp. 22-37, 2014.
- [119] X. Guo and H. Gao, "Bio-inspired material design and optimization," in *IUTAM Symposium on Topological Design Optimization of Structures, Machines and Materials: Status and Perspectives*, M. P. Bendsøe, N. Olhoff, and O. Sigmund, Eds., ed Dordrecht: Springer Netherlands, pp. 439-453, 2006.
- [120] F. Barthelat, A. K. Dastjerdi, and R. Rabiei, "An improved failure criterion for biological and engineered staggered composites," *Journal of The Royal Society Interface*, vol. 10, 2012.
- [121] A. G. Evans, Z. B. Ahmad, D. G. Gilbert, and P. W. R. Beaumont, "Mechanisms of toughening in rubber toughened polymers," *Acta Metallurgica*, vol. 34, pp. 79-87, 1986.

- [122] R. Rabiei, "Deformation and fracture of mineralized biological materials," Doctor of Philosophy Thesis, Department of Mechanical Engineering, McGill University, 2011.
- [123] S. Bekah, R. Rabiei, and F. Barthelat, "Structure, scaling, and performance of natural micro- and nanocomposites," *BioNanoScience*, vol. 1, pp. 53-61, 2011.
- [124] M. F. Ashby, "Overview no. 80: on the engineering properties of materials," *Acta Metallurgica*, vol. 37, pp. 1273-1293, 1989.

## APPENDICES

### Appendix A

Sample code for Toughness waviness model

```
close all

clear

clc

% This code is used to calculate the R curve for nacre
% considering waviness

% yp=dw/da

%UB + LB + 4 experimental values

L=5e-3; %mm

t=0.5e-3; %mm

angle=5*pi/180; %rad

h=30e-6; %mm

taus=25; %MPa

Lo=0.1*L; %mm

Gi=1.4e3; %MPa

Et=100e3; %MPa

Lc=L-Lo;

% Elastic Modulus

vf=t/(2*t+h);
```

```

cf2=vf*(Et*h*t)/(Et*h*t+Lc*Gi*(Lo-h*angle));
E=cf2*Gi*L*(Lo-h*angle)/(t*h)
S=Lo/(t+h)*taus
sty_max=0.008;
sty_el=0.001;
umax=L*sty_max;
us=L*sty_el;
stx_max=Lo*angle/(h+t);
sty_max=umax/L;
sigx=(us-Lo)/Lc*taus*sin(angle);
sigy=(Lo-us)/t*taus*cos(angle);
stxr=stx_max-sigx/E;
styr=sty_max-sigy/E;
c=0.06;

alpha=c*E/S^2*(sigx*stxr+sigy*styr)
Jb=0.5*L/t*taus*umax;

odeWake = @(t,J,yp) [2*J*alpha*((1+yp)*sqrt(1+2*yp))/yp-
yp*acot(yp/sqrt(1+2*yp))-
(1+2*yp)^(3/2)*log((1+2*yp)/(1+yp))/yp^2)-J+Jb]
t0 = pi/2;

```

```

y0 = 0;
yp0 = 1;
[y0,yp0]= decic(odeWake,t0,y0,0,yp0,1)
lamda=pi/8*Jb*E/S^2
tspan = [lamda 0.2];
[t,y] = ode15i(odeWake, tspan, y0,yp0)
Jt=1/c*S^2*y/E; % where y is w wake width which increase
with crack extension
plot(t,Jt,'*')
odeWake1 = @(t,J,yp) [2*J*alpha*((1+yp)*sqrt(1+2*yp)/yp-
yp*acot(yp/sqrt(1+2*yp)) -
(1+2*yp)^(3/2)*log((1+2*yp)/(1+yp))/yp^2)-J+(t/lamda*(Jb))]
tspan1 = [0 lamda];
y01= 0;
yp01 = 1;
[y0,yp0]= decic(odeWake,t0,y01,0,yp01,1)
[t1,y1] = ode15i(odeWake1, tspan1, y01,yp01)
Jt1=1/c*S^2*y1/E;

L=10e-3; %mm
t=0.4e-3; %mm
angle=5*pi/180; %rad

```

```

h=20e-6; %mm
taus=37; %MPa
Lo=0.5*L; %mm
Gi=1.4e3; %MPa
Et=100e3; %MPa
Lc=L-Lo;

% Elastic Modulus
vf=t/(2*t+h);
cf2=vf*(Et*h*t)/(Et*h*t+Lc*Gi*(Lo-h*angle));
E=cf2*Gi*L*(Lo-h*angle)/(t*h)
S=Lo/(t+h)*taus
sty_max=0.015;
sty_el=0.001;
umax=L*sty_max;
us=L*sty_el;
stx_max=Lo*angle/(h+t);
sty_max=umax/L;
sigx=(us-Lo)/Lc*taus*sin(angle);
sigy=(Lo-us)/t*taus*cos(angle);
stxr=stx_max-sigx/E;
styr=sty_max-sigy/E;
c=0.06;

```

```

alpha=c*E/S^2*(sigx*stxr+sigy*styr)
Jb=0.5*L/t*taus*umax;

odeWake = @(t,J,yp) [2*J*alpha*((1+yp)*sqrt(1+2*yp)/yp-
yp*acot(yp/sqrt(1+2*yp)) -
(1+2*yp)^(3/2)*log((1+2*yp)/(1+yp))/yp^2)-J+Jb]
t0 = pi/2;
y0 = 1;
yp0 = 1;
[y0,yp0]= decic(odeWake,t0,y0,0,yp0,1)
lamda=pi/8*Jb*E/S^2
tspan = [lamda 0.7];
[t,y] = ode15i(odeWake, tspan, y0,yp0)
Jt=1/c*S^2*y/E; % where y is w wake width which increase
with crack extension
% plot(t,Jt, '*')
odeWake1 = @(t,J,yp) [2*J*alpha*((1+yp)*sqrt(1+2*yp)/yp-
yp*acot(yp/sqrt(1+2*yp)) -
(1+2*yp)^(3/2)*log((1+2*yp)/(1+yp))/yp^2)-J+(t/lamda*(Jb))]
tspan1 = [0 lamda];
y01= 0;
yp01 = 1;

```

```

[t1,y1] = ode15i(odeWake1, tspan1, y01,yp01)
Jt1=1/c*S^2*y1/E;

hold on
plot(t,Jt,'<',t1,Jt1,'<')

hold on

xlabel('crack extention (mm)')
ylabel('Toughness J(kJ/m2)')

grid%

%%%%%%%%%%%% running my code with experimental values

c=0.06;

a=1.5;

S=70;

E=80e3;

stmax=0.015;

alpha=c*(E*stmax/S-1)

Jo=0.3;

Jb=12e-3+Jo;

odeWake = @(t,J,yp) [2*J*alpha*((1+yp)*sqrt(1+2*yp))/yp-
yp*acot(yp/sqrt(1+2*yp))-
(1+2*yp)^(3/2)*log((1+2*yp)/(1+yp))/yp^2)-J+(Jb)]

t0 = pi/2;

```

```

y0 = 1;
yp0 = 1;
lamda=pi/8*Jb*E/S^2
tspan = [lamda 0.8]; % lamda=0.1
[t,y] = ode15i(odeWake, tspan, y0,yp0)
Jt=1/c*S^2*y/E; % where y is w wake width which increase
with crack extension
plot(t-a,Jt)
hold on
xlabel('crack extention (mm)')
ylabel('Toughness J(kJ/m2)')
grid

%%%%%%%%%%%%%%%%%%%%%%%%%%%%%%%%%%%%%%%%%%%%%%%%%%%%%%%%%%%%%%%%%%%%%%%%
%%%%%%%%
% toughness amplification paper experimental results
reproduced

x1=[0 0.018 0.032 0.048 0.07 0.102 0.136 0.166];
y1=[0.05 0.07 0.095 0.12 0.158 0.21 0.315 0.425];
x2=[0 0.001 0.03 0.038 0.062 0.093 0.122 0.156 0.184];
y2=[0.06 0.08 0.115 0.14 0.17 0.24 0.285 0.36 0.44];
% an experimental investigation o d

```

```

x3=[0 0 0 0.02 0.03 0.03 0.03 0.034 0.063 0.063 0.07 0.076
0.093 0.103 0.12 0.133 0.16 0.17 0.186 0.197 0.215 0.255
0.283 0.347 0.53];
y3=[0.15 0.24 0.30 0.38 0.49 0.52 0.58 0.6 0.62 0.695 0.74
0.78 0.83 0.85 0.92 0.97 1.03 1.06 1.11 1.16 1.22 1.29 1.33
1.41 1.57 ];

x4=[0 0 0 0.015 0.03 0.058 0.058 0.085 0.085 0.105 0.12
0.125 0.165 0.165 0.19 0.23 0.28 0.315 0.37 0.4 0.45];
y4=[0 0.065 0.13 0.33 0.49 0.52 0.58 0.62 0.67 0.7 0.76 0.8
0.875 0.91 0.96 1 1.06 1.12 1.16 1.21 1.25];
plot(x1,y1,'s',x2,y2,'^',x3,y3,'o',x4,y4,'d')
axis([0,0.55,0,3])
grid on

legend('Lower Bound', 'Upper bound', 'Upper
bound', 'toughness model', 'Rabiei et al. 1', 'Rabiei et al.
2', 'Barthelat 1', 'Barthelat 2')

```

## Appendix B

### Optimization Sample Code

#### Define Functions

```
function f=ESJCS(x) % f has 3 columns
% x is a vectore (L,t,theta,Lo,h,Gi,taus)

% numObj = 2;
% m = size(x,1);
% % f = zeros(m,numObj);

L=x(1)/100;
t=x(2)/100;
theta=x(3)*pi/180;
h=x(4)/1000;
Lo=x(5)/100;
taus=x(6);
Gi=x(7);
Et=x(8)*1000;

% first Objective function
vf=t/(2*t+h);

Lc=L-Lo;

cf2=vf*(Et*h*t)/(Et*h*t+Lc*Gi*(Lo-h*theta));
E=-cf2*Gi*L*(Lo-h*theta)/(t*h);
```

```

% % second Objective function
sigs=-Lo/(t+h)*taus;

% Third Objective function
sty_max=1;%mm
sty_el=0.1;%mm
umax=L*sty_max;
us=L*sty_el;
stx_max=Lo*theta/(h+t);
sty_max=umax/L;
sigx=(us-Lo)/Lc*taus*sin(theta);
sigy=(Lo-us)/t*taus*cos(theta);
En=-E;

stxr=stx_max-sigx/En;
styr=sty_max-sigy/En;
z=(0.066*En/(sigs)^2)*(sigx*stxr+sigy*styr);
Jb=0.5*taus*umax*L/t;

if z<0 || z>=0.9
    z=0;
end

J=-Jb/(1-z); %<- 3rd objective function
f=[E J sigs]';

end

```

## Constraints

```
function [C, Ceq] = mynonlconESJCS(x)

L=x(1)/1000; % micrometer
t=x(2)/1000; % micrometer
theta=x(3)*pi/180;
h=x(4)/1000; %micrometer
Lo=x(5)/1000; %micrometer
taus=x(6); %MPa
Gi=x(7); %MPa
Et=x(8)*1000; %GPa
% taus=10;%MPa
% Gi=6.3;%Mpa
% Kic=0.5*10^(3/2); %MPa*mm^0.5
Kic=1.2*10^(3/2); %MPa*mm^0.5
dd=0;
C(1,1)=(L/t-0.56*Kic/(taus*sqrt(t)))-dd;
C(2,1)=(sqrt(3)-Lo/(t+h))-dd;
C(3,1)=(Lo/L-0.5)-dd;
Ceq=[];
```

## Output function

```

function [state, options,optchanged] =
outputfunction(options,state,flag)

%displays the function eval value at each iteration. You
can change this
disp(state.FunEval);

optchanged = false;

switch flag
    case 'init'
        disp('Starting the algorithm');
    case {'iter','interrupt'}
        disp('Iterating ...')
    case 'done'
        disp('Performing final task');
end

my view function

function [state, options,optchanged] =
my_view(options,state,flag,interval)

% function to view the population

optchanged = false;

if flag=='init'
    disp('Population at the start of the algorithm');
    disp(state.Population)

```

```
end
```

```
end
```

### Run MultiObjective

```
clear
```

```
close all
```

```
clc
```

```
nvars = 8;
```

```
% L=x(1);t=x(2);theta=x(3); h=x(4);Lo=x(5);taus=x(6);
```

```
Gi=x(7);Et=x(8)
```

```
% bounds
```

```
lb = [1 1 0 1 1 1 1 1]; %0.001mm=1um
```

```
ub = [100 100 5 50 100 50 50 11]*10; % 5/180*pi=0.0873
```

```
% Inequality Constraints
```

```
Aineq=[-1 1 0 0 0 0 0 0
```

```
        -1 0 0 0 1 0 0 0];
```

```
bineq=[0 0]';
```

```
% Equality Constraints
```

```
Aeq=[];
```

```
beq=[];
```

```
% Defining Options
```

```

options =
gaoptimset('PopulationSize',400,'Generations',500,'PlotFcns',@gaplotpareto,'display','iter','TolFun',1e-
6,'TolCon',1e-3,'OutputFcns',@my_view);
options.DistanceMeasureFcn =
{@distancecrowding,'genotype'};
% Multi Objective Optimization
[x,fval,exitFlag,output,population,scores] =
gamultiobj(@ (x) ESJCS(x),nvars,Aineq,bineq,Aeq,beq,lb,ub,@ (x)
)myonlconESJCS(x),options);
% Stiffness E, toughness J, Strength S
Efv=-fval(:,1);
Jfv=-fval(:,2);
Sfv=-fval(:,3);
% 3D plot of Stiffness E, toughness J & Strength S
plot(Efv,Jfv,'+')
xlabel('E (MPa)')
ylabel('J (kg/m2)')
% Saving data to a file
save DVCS11 x Efv Sfv Jfv

```

**Run Results**

```

clear

```

```

close all

clc

% loading data
d=load('DVCS11.mat');

x=d.x;

n=length(x);

L=x(:,1)/1000;

t=x(:,2)/1000;

h=x(:,4)/1000;

theta=x(:,3)*pi/180;

Lo=x(:,5)/1000;

taus=x(:,6);

Gi=x(:,7);

Et=x(:,8)*1000;

E=d.Efv;

J=d.Jfv;

S=d.Sfv;

% Reshape data into matrix

Ep=reshape(E,10,14);

Jp=reshape(J,10,14);

Sp=reshape(S,10,14);

% plotting stem

```

```
figure
stem3(Ep, Sp, Jp)
zlabel('J (kJ/m2)')
ylabel('S (MPa)')
xlabel('E (MPa)')
```